A GUIDANCE AND CONTROL STUDY FOR A LONG-RANGE AIR-TO-AIR MISSILE

A THESIS SUBMITTED TO
THE GRADUATE SCHOOL OF NATURAL AND APPLIED SCIENCES
OF
MIDDLE EAST TECHNICAL UNIVERSITY

BY

BURAK CAN KARABAĞ

IN PARTIAL FULFILLMENT OF THE REQUIREMENTS
FOR
THE DEGREE OF MASTER OF SCIENCE
IN
MECHANICAL ENGINEERING

SEPTEMBER 2024

Approval of the thesis:

A GUIDANCE AND CONTROL STUDY FOR A LONG-RANGE AIR-TO-AIR MISSILE

submitted by **BURAK CAN KARABAĞ** in partial fulfillment of the requirements for the degree of **Master of Science in Mechanical Engineering, Middle East Technical University** by,

Prof. Dr. Naci Emre Altun
Dean, **Graduate School of Natural and Applied Sciences** _____

Prof. Dr. Serkan Dağ
Head of the Department, **Mechanical Engineering** _____

Assist. Prof. Dr. Hakan Çalışkan
Supervisor, **Mechanical Engineering, METU** _____

Prof. Dr. M. Kemal Özgören
Co-Supervisor, **Mechanical Engineering, METU** _____

Examining Committee Members:

Prof. Dr. Yiğit Yazıcıoğlu
Mechanical Engineering, METU _____

Assist. Prof. Dr. Hakan Çalışkan
Mechanical Engineering, METU _____

Prof. Dr. Ender Ciğeroğlu
Mechanical Engineering, METU _____

Assoc. Prof. Dr. Ali Emre Turgut
Mechanical Engineering, METU _____

Assist. Prof. Dr. Yakup Özkazanç
Electrical and Electronics Eng., Hacettepe Uni. _____

Date: 03.09.2024

I hereby declare that all information in this document has been obtained and presented in accordance with academic rules and ethical conduct. I also declare that, as required by these rules and conduct, I have fully cited and referenced all material and results that are not original to this work.

Name Last name : Burak Can Karabağ

Signature :

ABSTRACT

A GUIDANCE AND CONTROL STUDY FOR A LONG-RANGE AIR-TO-AIR MISSILE

Karabağ, Burak Can
Master of Science, Mechanical Engineering
Supervisor : Assist. Prof. Dr. Hakan Çalışkan
Co-Supervisor: Prof. Dr. M. Kemal Özgören

September 2024, 93 pages

In the guidance and control area, the pursuit of a highly maneuverable evasive airborne target by an air-to-air missile through a long range is a challenging problem. For the air-to-air missiles, precision is an important requirement. The impact time and velocity should also be taken into consideration in the case of long ranges. In this thesis, a hybrid guidance law consisting of an optimal midcourse phase and a terminal phase with standard Proportional Navigation Guidance (PNG) is proposed for a beyond-visual-range air-to-air missile. The midcourse phase of the proposed guidance law is posed and solved as an optimal control problem. In the optimal midcourse phase, the impact time is minimized through nonlinear programming via the direct collocation method. The transition from the midcourse to the terminal phase is described as entering a sphere around the target, which has an appropriately predetermined radius for an effective terminal phase. Optimization of the midcourse phase also considers the terminal phase. It provides an optimal entrance point to the mentioned sphere with an optimal Line-of-Sight (LOS) angle. Entering through this point as such means minimizing maneuvers and acceleration demands of the missile.

Moreover, the proposed guidance law considers the limits of the physical parameters such as angle of attack and fin deflections as well and keeps them within the limits by formulating them as path constraints in the problem. The performance of the proposed guidance law is assessed by means of several simulations of different interception scenarios.

Keywords: Beyond Visual Range Air-To-Air Missile, Ramjet Propulsion, Optimal Midcourse Guidance, Nonlinear Programming, Path Constraints

ÖZ

UZUN MENZİLLİ BİR HAVA-HAVA FÜZESİ İÇİN GÜDÜM-KONTROL ÇALIŞMASI

Karabağ, Burak Can
Yüksek Lisans, Makina Mühendisliği
Tez Yöneticisi: Dr. Öğr. Üyesi Hakan Çalışkan
Ortak Tez Yöneticisi: Prof. Dr. M. Kemal Özgören

Eylül 2024, 93 sayfa

Güdüm kontrol alanında, yüksek manevra kabiliyetine sahip, kaçınma manevraları yapabilen hava hedeflerinin bir hava-hava füzesiyle uzun menzilden vurulması zorlu bir problemdir. Hava-hava füzeleri için vuruş hassasiyeti önemli bir gerekliliktir. Uzun mesafelerde uçuş süresi ve vuruş enerjisi (hız) de dikkate alınmalıdır. Böyle bir füzenin yukarıda belirtilen gerekliliklerinin karşılanması için güdüm komutlarının oluşturulmasına yönelik uygun güdüm yöntemlerine ihtiyaç duyulmaktadır. Bu tezde, "görüş ötesi menzilli" hava-hava füzeleri için, optimal bir ara faz aşaması ve standart oransal seyir güdümü ile bir terminal aşamasından oluşan yeni bir hibrit güdüm kuralı önerilmektedir. Önerilen güdüm kuralının ara fazı, bir optimal kontrol problemi olarak ortaya konmuş ve çözülmüştür. Optimal ara faz aşamasında, doğrusal olmayan programlama yolu ve doğrudan sıralamayla uçuş süresi en aza indirilmiştir. Ara fazdan terminal güdüm aşamasına geçiş, önceden belirlenmiş bir yarıçapa sahip olan hedefin etrafındaki bir küreye girmek olarak tanımlanabilir. Ara faz aşamasının optimizasyon süreci aynı zamanda terminal güdüm aşamasına geçişi de dikkate almaktadır. Optimal görüş hattı açısıyla söz konusu küreye optimal giriş noktası sağlamaktadır. Bu noktadan giriş, füzenin geçiş

anındaki manevra ve ivme taleplerinin en aza indirilmesi, dolayısıyla sürenin kısaltılması ve terminal aşamasında hedefi vurma olasılığının artması anlamına gelmektedir. Ayrıca önerilen güdüm kuralı, kanatçık sapmaları ve hücum açısı gibi fiziksel parametrelerin sınırlarını da dikkate almakta ve bunları problemdeki yörünge kısıtları olarak formüle ederek sınırlar içinde tutmaktadır. Tasarlanan güdüm kuralının performansı, farklı angajman senaryolarının çeşitli simülasyonları aracılığıyla değerlendirilirmiştir.

Anahtar Kelimeler: Görüş Ötesi Menzilli Hava-Hava Füzesi, Ramjet ile İtki, Optimal Ara Faz Güdümü, Doğrusal Olmayan Programlama, Yörünge Kısıtları

Youth of Türkiye’s future! Even in such worst circumstances, it is your duty to save the Turkish Independence and Republic. You will find the strength you need in your noble blood.

Mustafa Kemal ATATÜRK

ACKNOWLEDGMENTS

First, I would like to express my gratitude to my supervisor, Assist. Prof. Dr. Hakan ÇALIŞKAN, for giving me the opportunity to work in the guidance and control field and for his understanding and support. I would also like to express my gratitude to my co-supervisor, Prof. Dr. M. Kemal ÖZGÖREN, from the bottom of my heart for his invaluable advice, confidence, and encouragement. I consider it an honor for me to work with him, and I could not finish this thesis without him.

I am grateful to Dr. Kadriye TİRYAKİ KUTLUAY for her inspiration and visionary guidance in supporting this thesis to be accomplished. Also, I would like to mention Muharrem ULU for his valuable discussions on the thesis subject for long hours and technical insight he shared with me. This thesis cannot be successfully finished without his suggestions and never-ending encouragement.

Furthermore, I would like to thank all my colleagues at TÜBİTAK SAGE for their motivation and understanding.

Above all else, I want to thank my mother Handan GÜVENÇALAN and her family, my grandmother Sevim YEMEN, my uncle H. Bülent GÜVENÇALAN, my aunts Canan GÜVENÇALAN and Kezban GÜVENÇALAN, for all they have done to raise me and get me to this point in my life. Their sacrifices are unrepayable.

Lastly and certainly at the top, I am forever thankful to the love of my life, Ezgi ÇETİNKAYA, for all the love, patience and support she has given to me. We have prevailed over all challenges as a team.

TABLE OF CONTENTS

ABSTRACT v

ÖZ vii

ACKNOWLEDGMENTS x

TABLE OF CONTENTS xi

LIST OF TABLES xiii

LIST OF FIGURES xiv

LIST OF ABBREVIATIONS xvi

LIST OF SYMBOLS xvii

CHAPTERS

1 INTRODUCTION 1

1.1 Introduction 1

1.2 Literature Review 4

1.3 Contributions 7

1.4 Thesis Outline 8

2 MATHEMATICAL WORK 11

2.1 Mathematical Model of the Missile 11

2.1.1 Missile Modelled as a Particle 11

2.1.2 Thrust Model 24

2.1.3 Aerodynamical Model of the Missile 28

2.1.4 Roll Autopilot 34

2.1.5 Control Actuation System 38

2.2 Mathematical Model of the Target 40

3 GUIDANCE METHODS 43

3.1 Optimal Midcourse Guidance 44
3.1.1 Definitions of Optimal Control Problem 45
3.1.2 Direct Collocation Method 47
3.1.3 Trapezoidal Discretization 48
3.1.4 Constraints 49
3.1.5 Interpolation 50
3.1.6 Formulation of Trajectory Optimization 52
3.2 Standart Proportional Navigation Guidance – Terminal Phase 55
3.3 Reference Guidance Law – PN Guidance with Lofting 58
4 SIMULATION WORK 61
4.1 Case 1 – Nonmoving Target Engagement 63
4.2 Case 2 – Turn and Run Engagement 68
4.3 Case 3 – Head-On Engagement 73
4.4 Case 4 – Tail-Chase Engagement 77
5 CONCLUSION AND FUTURE WORKS 83
5.1 Conclusion 83
5.2 Future Works 87
REFERENCES 89

LIST OF TABLES

TABLES

Table 2.1 Physical Parameters of the Missile 28
Table 2.2 Roll Position Autopilot Metrics 37
Table 3.1 Upper and Lower Bounds for the States of the Missile 52
Table 3.2 “fmincon” Options Used in Simulations 54
Table 4.1 Initial Conditions of Case 1 – Nonmoving Target Engagement 63
Table 4.2 Results of Nonmoving Target Engagement Simulation 67
Table 4.3 Initial Conditions of Case 2 – Turn and Run Engagement 68
Table 4.4 Results of Turn and Run Engagement Simulation 72
Table 4.5 Initial Conditions of Case 3 – Head-On Engagement 73
Table 4.6 Results of Head-On Engagement Simulation 77
Table 4.7 Initial Conditions of Case 4 – Tail-Chase Engagement 77
Table 4.8 Results of Tail-Chase Engagement Simulation 81

LIST OF FIGURES

FIGURES

Figure 1.1 AIM-120 AMRAAM [2] 2
Figure 1.2 Vympel R-77 [3] 2
Figure 1.3 PL-15 Missile [4] 3
Figure 1.4 Meteor Missile [1] 3
Figure 2.1 Relation between Body-Fixed and Wind Frames 13
Figure 2.2 Representation of Frames used in Modeling Work 13
Figure 2.3 Side View of the Missile 21
Figure 2.4 Specific Impulse of Various Jet Engines [19] 26
Figure 2.5 Control Derivative of Lift Force Coefficient vs Elevator Deflections 31
Figure 2.6 AoA Stability Derivative of Lift Force Coefficient vs AoA 32
Figure 2.7 Actual and Fitted $C_{L\delta e}$ vs Mach Number 33
Figure 2.8 Actual and Fitted $C_{L\alpha}$ vs Mach Number 33
Figure 2.9 Roll Rate and Position Feedback Loops [23] 34
Figure 2.10 Root Locus Diagram of Roll Autopilot [23] 35
Figure 2.11 Step Response of the Roll Autopilot 37
Figure 2.12 Step Response of the Aileron Deflection Command 38
Figure 2.13 X Configuration of Fins [25] 39
Figure 3.1 Typical Guidance Phases of a BVRAAM [31] 44
Figure 3.2 Function Approximation Using a Linear Spline [26] 50
Figure 3.3 Illustration of the Linear and Quadratic Spline Segments [26] 51
Figure 3.4 Function Approximation using a Quadratic Spline [26] 51
Figure 3.5 Sketch of a Simple Engagement with PNG [32] 56
Figure 4.1 Elevational Acceleration of the Missile vs Time – Nonmoving 64
Figure 4.2 Lateral Acceleration of the Missile vs Time – Nonmoving 64
Figure 4.3 Altitude of the Missile vs Time – Nonmoving 65
Figure 4.4 y Position vs x Position of the Missile – Nonmoving 65
Figure 4.5 Angle of Attack vs Time – Nonmoving 66

Figure 4.6 Fin Deflection Angles vs Time – Nonmoving..... 66
Figure 4.7 3D Trajectory of the Missile – Turn and Run 68
Figure 4.8 Altitude of the Missile vs Time – Turn and Run..... 69
Figure 4.9 Elevational Acceleration of the Missile vs Time – Turn and Run 69
Figure 4.10 Lateral Acceleration of the Missile vs Time – Turn and Run 70
Figure 4.11 Speed of the Missile vs Time – Turn and Run 70
Figure 4.12 Angle of Attack vs Time – Turn and Run 71
Figure 4.13 Fin Deflection Angles vs Time – Turn and Run 71
Figure 4.14 3D Trajectory of the Missile – Head-On..... 73
Figure 4.15 Altitude of the Missile vs Time – Head-On 74
Figure 4.16 Elevational Acceleration of the Missile vs Time – Head-On..... 74
Figure 4.17 Lateral Acceleration of the Missile vs Time – Head-On..... 75
Figure 4.18 Speed of the Missile vs Time – Head-On..... 75
Figure 4.19 Angle of Attack vs Time – Head-On..... 76
Figure 4.20 Fin Deflection Angles vs Time – Head-On..... 76
Figure 4.21 3D Trajectory of the Missile and the Target – Tail-Chase..... 78
Figure 4.22 Altitude of the Missile vs Time – Tail-Chase..... 78
Figure 4.23 Elevational Acceleration of the Missile vs Time – Tail-Chase..... 79
Figure 4.24 Lateral Acceleration of the Missile vs Time – Tail-Chase..... 79
Figure 4.25 Speed of the Missile vs Time – Tail-Chase..... 80
Figure 4.26 Angle of Attack vs Time – Tail-Chase..... 80
Figure 4.27 Fin Deflection Angles vs Time – Tail-Chase..... 81

LIST OF ABBREVIATIONS

ABBREVIATIONS	
AAM	Air-to-Air Missile
BVRAAM	Beyond-Visual-Range Air-to-Air Missile
BTT	Bank-to-Turn Flight Maneuver
PNG	Proportional Navigation Guidance
BVR	Beyond Visual Range
LOS	Line Of Sight
ENU	East-North-Up Reference Frame Fixed to Earth
CAS	Control Actuation System
ICAO	International Civil Aviation Organization
DOF	Degree of Freedom
AoA	Angle of Attack
INS	Inertial Navigation System

LIST OF SYMBOLS

SYMBOLS

t	Time (s)
m	Mass of missile (kg)
J_1, J_2, J_3	Princip. moments of inertia about x, y, z axes (kgm^2)
g	Gravitational acceleration (m/s^2)
$\mathcal{F}_e, \mathcal{F}_w, \mathcal{F}_b$	ENU (East-North-Up), Wind, and Body Frames $(-)$
x_m, y_m, z_m	x, y, z coordinates of missile in ENU frame (m)
V_m	Velocity of missile (m/s)
γ_m, η_m	Elevation and azimuth angles of missile velocity (°)
a_γ, a_η	Elevational and Azimuthal acc. commands (m/s^2)
x_t, y_t, z_t	x, y, z coordinate of target in ENU frame (m)
V_t	Velocity of target (m/s)
γ_t, η_t	Elevation and azimuth angles of target velocity (°)
$\hat{C}^{(e,w)}$	Transformation matrix from Wind to ENU frame $(-)$
$\hat{C}^{(w,b)}$	Transformation matrix from Body to Wind frame $(-)$
$\hat{R}$	Rotation matrix (-)
$e^{\tilde{n}a}$	Exponential expression of rotation matrix $(-)$
$\vec{u}_1, \vec{u}_2, \vec{u}_3$	Basis vectors of a frame $(-)$
$\bar{u}_1, \bar{u}_2, \bar{u}_3$	Column matrix representations of basis vectors $(-)$
$\tilde{u}_1, \tilde{u}_2, \tilde{u}_3$	Skew symmetric cross product matrices $(-)$

φ_m	Bank angle of missile (°)
θ, ϕ, ψ	Pitch, roll and yaw (Euler) angles of missile (°)
α, β	Angle of attack and side slip angle (°)
$\delta_e, \delta_r, \delta_a$	Elevator, rudder, and aileron deflections (°)
$\delta_1, \delta_2, \delta_3, \delta_4$	Fin deflections (°)
I_{sp}	Specific impulse of ramjet motor (s)
T, S, D, L	Thrust, side, drag and lift forces acting on missile (N)
C_D, C_L	Drag and lift force coefficients $(-)$
$C_{D,0}$	Zero-lift drag force coefficient $(-)$
L_α, L_{δ_e}	Stability and control derivatives of lift force (N)
ρ	Air density (kg/m^3)
Q_d	Dynamic pressure at a specific speed (Pa)
L_{Ref}	Aerodynamical reference length of missile (m)
S_{Ref}	Aerodynamical reference area of missile (m^2)
e	Oswald efficiency factor $(-)$
AR	Aspect ratio of the missile $(-)$
J	Objective function of optimal control problem (s)
C_{l_p}	Aerodyn. coefficient of roll damping derivative $(-)$
$C_{l_{\delta_a}}$	Aerodyn. coefficient of roll control derivative $(-)$
$M_{lp}, M_{l\delta_a}$	Roll moment damping and control derivatives $(-)$
ζ	Damping ratio of roll autopilot $(-)$

ω_n	Natural frequency of roll autopilot (rad/s)
K_ϕ	Roll control angular position feedback gain $(-)$
K_p	Roll control angular velocity feedback gain $(-)$
ζ_{CAS}	Damping ratio of control actuation system $(-)$
$\omega_{n,CAS}$	Natural frequency of control actuation sys (rad/s)
x	Array of state variables in optimal control prob. $(-)$
u	Array of control inputs in optimal control prob. $(-)$

CHAPTER 1

INTRODUCTION

1.1 Introduction

Beyond-visual-range-air-to-air-missiles (BVRAAM) have a crucial role in modern air-to-air warfare. These missiles have the capability to detect the target using radar or other sensor systems, without requiring direct visual contact with enemy aircraft. BVRAAMs allow shooter platforms to execute efficient assaults without the need to approach air defense systems of enemies. Therefore, it is crucial to achieve air dominance.

BVRAAMs need to possess high speed, extensive operational range, and remarkable guidance precision. BVRAAMs frequently contain active radar seekers equipped with radar transceivers and essential electronics to independently detect and track a target. A data link exists between the launch platform and the missile. Through the use of this datalink, the shooter aircraft transmits target position updates obtained from its radar to the missile until the missile transitions into an active state. This indicates that the missile's active radar seeker is able to independently detect and track the target. Once the missile becomes active, there is no requirement to provide target updates via datalink. This feature is referred to as 'fire and forget', as it allows the shooter aircraft to engage other targets or leave from the area after launching the missile.

Several nations worldwide are allocating resources to acquire BVRAAM systems in

order to enhance the capabilities of their air forces. Here are some examples of missiles:

- The AIM-120 AMRAAM is utilized in several airplanes, including the F-15, F-16, F/A-18, and F-22, by the United States.



Figure 1.1 AIM-120 AMRAAM [2]

- Russia incorporates the Vympel R-77 with Su-27, MiG-29, and Su-35 aircrafts.

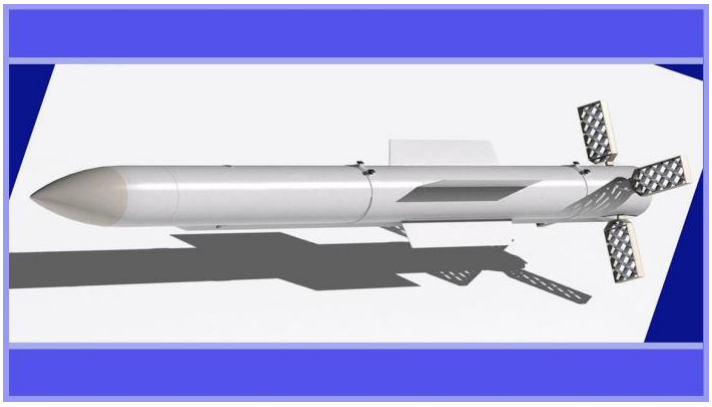


Figure 1.2 Vympel R-77 [3]

- China has successfully integrated PL-12 and PL-15 missiles into advanced fighter aircraft including J-10, J-11, and J-20.



Figure 1.3 PL-15 Missile [4]

- MBDA Meteor, a European weapon system, is employed in many aircraft models including the Eurofighter Typhoon, Dassault Rafale, and Saab Gripen.



Figure 1.4 Meteor Missile [1]

BVRAAMs are employed to establish air dominance, safeguard critical strategic elements, and destroy any hostile airborne dangers. These missiles play a crucial role in both defensive and offensive doctrines.

1.2 Literature Review

There is a substantial body of research results in the literature focused on the optimization of trajectories for air-to-air missiles. Significant research has been conducted to enhance the guidance capabilities of these missiles using optimal control theory and singular perturbation method. Some of the prominent research samples are indicated below.

In their 1979 study, Goldstein and Calise examined the integration of guidance and propulsion systems in air-to-air missiles using ramjet engines. They demonstrated that optimal control approaches can significantly enhance the effectiveness of missile guidance systems. This work aims to achieve optimal aerodynamic and propulsion control of the missile through the utilization of singular perturbation methods. These strategies provide substantial computational benefits for assessing missile performance [5].

In Sarkar's (2011) study, the author utilized nonlinear programming techniques to optimize missile guidance systems and determine the trajectory that would result in the longest flight range for air-to-air missiles. The work successfully solved the trajectory shaping problem by utilizing the direct transcription method and optimal control theory. Subsequently, the optimization outcomes obtained in this investigation were inputted into the simulation environment with six degrees of

freedom, and the findings were evaluated in the model that closely resembles the real world [6].

The study conducted by Hong, Tahk, and Lee (2019) focused on the examination of tactical guidance rules and stage optimization techniques for anti-air missiles. The launch and intermediate phase components of the guidance algorithm have been optimized using stage optimization techniques. While the applied method results in a small decline in system performance compared to traditional optimizations, it offers crucial insights into establishing the necessary phase weights for a practical missile system [7].

In literature, there are also methods used for guidance studies other than optimal control theory.

Reinforcement learning (RL) is another method used in guidance studies for BVRAAMs. It is a process of training an agent to make a series of decisions by providing rewards for desired behaviors and penalties for undesired behaviors. Van Hoorn's work (2019) focused on enhancing the guidance of air-to-air missiles through the application of reinforcement learning techniques. This study has established a guidance law that achieves performance similar to optimal guidance operations by utilizing deep reinforcement learning algorithms. Additionally, the guidance law also offers real-time feedback. The presented technique exhibits considerably inferior performance compared to optimal guidance, but superior performance compared to biased proportional navigation guidance [8].

Genetic Algorithm (GA) is an optimization technique that emulates the natural selection process to produce superior solutions for search and optimization problems.

Yang, Fang, and Qi (2005) introduced a sophisticated midcourse guidance method that relies on genetic algorithm (GA). The suggested midcourse guidance formulation aims to reduce the duration of the flight and optimize the terminal kinetic energy, while also satisfying a criterion for intercepting the target. Genetic algorithms (GA) are employed to determine optimal angle of attack for the flight trajectory. The optimal guidance method is produced by combining genetic algorithm (GA) with singular perturbation method (SPM). SPM is utilized to determine the final duration of the flight. This approach entirely obviates the necessity of addressing two-point boundary-value issues, which are commonly complex in terms of derivation and implementation. The simulation results demonstrate that the resulting guidance law is near optimal and valid, particularly in successfully intercepting movement targets [9].

Particle Swarm Optimization (PSO) is a computational technique that iteratively enhances potential solutions by leveraging the collective movement and intelligence of swarms. In their study, Lee et al. (2016) introduced a guidance system called the proportional navigation-improved particle swarm optimization guidance (PN-IPSOG). This system aims to enhance the performance of missile guidance. The IPSOG exhibits robustness and a fast reaction, but experiences instability during the initial phase. Hence, PN guidance is employed to initially modify the missile's attitude. Once the rate of the line-of-sight (LOS) angle becomes steady, the system transitions from PN guidance to IPSOG. The numerical simulation results demonstrate that the PN-IPSOG outperforms the conventional PN guidance in terms of miss distance and lateral accelerations, indicating greater precision and energy efficiency [10].

1.3 Contributions

The present study distinguishes itself from earlier studies by considering a greater number of restrictions that arise during flight and proposing a hybrid guidance rule that comprises proportional navigation guidance too in the terminal phase.

The primary contributions of the study can be explained below.

1. Optimization of Guidance Algorithms: Guidance algorithms are enhanced through the utilization of crucial data, including the target's location, velocity, and trajectory, provided by a ground station. This optimization allows missiles to efficiently and quickly reach their target with maximum kinetic energy.

2. Optimization Constraints: The optimization of the guidance algorithms considers hardware limitations. The flight performance criteria are achieved by adhering to limits such as fin deflections and the working envelope of the ramjet engine. Thus, the saturation of the control actuation system and the choking of the ramjet due to excessive angle of attack are prevented.

3. The transition from the optimal midcourse guidance mode to the terminal (PNG) guidance mode is done in a way that prevents high acceleration demands and avoids overloading the fins. It is achieved by entering the terminal mode at an optimal location with an optimal line-of-sight angle.

4. Maneuverability: Owing to the optimized midcourse phase, the missile possesses a high amount of kinetic energy during the terminal guidance phase, which allows it to execute agile maneuvers. Thus, it becomes capable of employing PNG effectively even to counter the target's last-ditch evasive maneuvers.

This study assumes that the mentioned data can be transmitted to the missile accurately in a consistent and uninterrupted manner from a ground station during the midcourse phase. During the terminal phase with PNG, the missile uses its own facilities, such as IMU and seeker.

1.4 Thesis Outline

This thesis comprises a mathematical representation of an BVRAAM, as well as the design of guidance system. Additionally, it includes a comparison of the derived guidance method with various interception scenarios.

- Chapter 1 provides an overview of AAMs and presents examples of them from different nations. It also includes a literature review and summarizes the scope of this thesis.

- Chapter 2 comprises modeling study. Within this section, the missile is represented as a particle. This section also encompasses the missile's subsystems, including the thrust model, roll autopilot and control actuation mechanism, as well as the aerodynamic model. In addition, this section contains the model that will be implemented to facilitate target movement in engagement scenarios.

- Chapter 3 encompasses the guidance methods employed in this thesis study. This section provides explanations for midcourse, terminal, and hybrid guidance. Detailed explanations are provided for the optimal control theory utilized in the midcourse phase of the proposed hybrid guidance method, as well as the standard proportional navigation (PN) guidance employed in the

terminal phase. The biased PN guidance, which is PN guidance with lofting method in simulation studies, is also elucidated to ensure a fair comparison.

- Chapter 4 comprises simulation studies involving typical engagement scenarios in air-to-air warfare. The studies have clearly proved the benefits of the proposed and presented guidance method.

Chapter 5 provides a summary of the outcomes of the thesis and offers suggestions for future research.

CHAPTER 2

MATHEMATICAL WORK

This chapter provides an explanation of the mathematical modeling of the missile and its subsystems, as well as the mathematical modeling of the target used in engagement scenarios.

2.1 Mathematical Model of the Missile

2.1.1 Missile Modelled as a Particle

2.1.1.1 Reference Frames and Transformation Matrices

In this part, three reference frames which are used in the modeling work are presented. All the frames are both orthogonal and right-handed.

- **Earth-Fixed East-North-Up Frame**

This is the absolute coordinate system fixed on the surface of the earth. It is used for expressing the motion of the missile and the target with respect to the earth.

This coordinate system is denoted as $\mathcal{F}_e = \mathcal{F}_e\left\{O;\ \vec{u}_1^{(e)}, \vec{u}_2^{(e)}, \vec{u}_3^{(e)}\right\}$. Its first, second, and third axes are aligned with the east, north, and up directions of the earth. Its origin O is a suitably selected fixed point on the earth.

- **Body-Fixed Frame**

The body-fixed frame $\mathcal{F}_b = \mathcal{F}_b\left\{C;\ \vec{u}_1^{(b)}, \vec{u}_2^{(b)}, \vec{u}_3^{(b)}\right\}$ is attached to the body of the missile and its origin C is the mass center of the missile.

The unit vector $\vec{u}_1^{(b)}$ is along the roll axis and it is oriented towards the front of the missile. The unit vector $\vec{u}_2^{(b)}$ is along the pitch axis, it is perpendicular to $\vec{u}_1^{(b)}$, and points to the left when the missile is viewed from the rear. The unit vector $\vec{u}_3^{(b)}$ is along the yaw axis and it is oriented in accordance with the right-hand rule.

- **Wind Frame**

The air mass can either be stationary or in motion (i.e., windy) relative to the earth. However, it is of course always in motion relative to the missile appearing as a relative wind. On the other hand, it is presumed that the air is monolithic, meaning that the air molecules continue to be adherent to each other. This property allows the air to be represented as a frame $\mathcal{F}_w = \mathcal{F}_w\left\{C;\ \vec{u}_1^{(w)}, \vec{u}_2^{(w)}, \vec{u}_3^{(w)}\right\}$. The origin C is taken as the mass center of the missile. Besides, the absolute velocity of the missile is very much higher than the velocity of the surrounding air. Therefore, the relative velocity of the missile with respect to the surrounding air is treated to be equal to its absolute velocity.

As the missile flies through the air, the relative wind that it encounters creates aerodynamic forces on its body.

The unit vectors of the wind frame are defined so that $\vec{u}_1^{(w)}$ is aligned with the whole velocity vector of the missile. The second one $\vec{u}_2^{(w)}$ is perpendicular to $\vec{u}_1^{(w)}$ and points towards the left when the missile is viewed from the rear. As for the third one $\vec{u}_3^{(w)}$, it is oriented by using the right-hand-rule.

The body-fixed frame $\mathcal{F}_b$ and the wind frame $\mathcal{F}_w$ are illustrated in Figures 2.1 and 2.2.

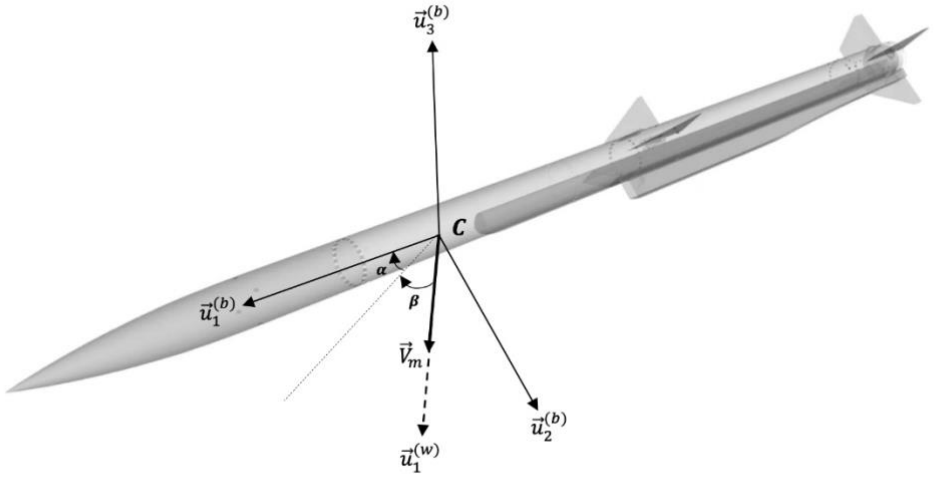


Figure 2.1 Relation between Body-Fixed and Wind Frames

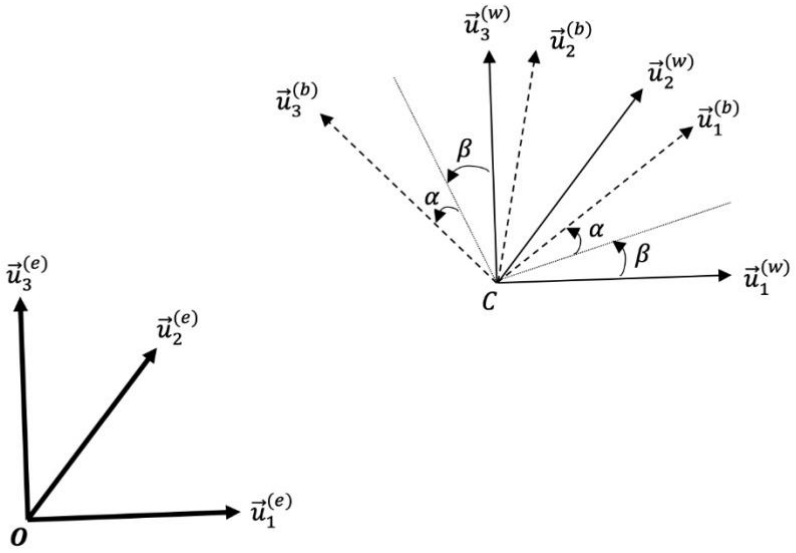


Figure 2.2 Representation of Frames used in Modeling Work

- **Rotation and Transformation of the Frames**

By using the Rodrigues' Formula and the exponential form of the rotation matrix [17], the basic rotation matrix can be expressed as follows for $k = 1, 2, 3$.

$$\widehat{R}_k(a) = \widehat{R}_k(\widetilde{u}_k, a) = e^{\widetilde{u}_k a} = \hat{I}\, cos(a) + \widetilde{u}_k\, sin(a) + \overline{u}_k \overline{u}_k^t (1 - cos(a)) \qquad (2.1)$$

The three basic rotation matrices are written out as shown below.

$$\widehat{R}_1(a) = \widehat{R}_1(\widetilde{u}_1, a) = e^{\widetilde{u}_1 a} = \begin{bmatrix} 1 & 0 & 0 \\ 0 & \cos(a) & -\sin(a) \\ 0 & \sin(a) & \cos(a) \end{bmatrix} \qquad (2.2)$$

$$\widehat{R}_2(a) = \widehat{R}_2(\widetilde{u}_2, a) = e^{\widetilde{u}_2 a} = \begin{bmatrix} \cos(a) & 0 & \sin(a) \\ 0 & 1 & 0 \\ -\sin(a) & 0 & \cos(a) \end{bmatrix} \qquad (2.3)$$

$$\widehat{R}_3(a) = \widehat{R}_3(\widetilde{u}_3, a) = e^{\widetilde{u}_3 a} = \begin{bmatrix} \cos(a) & -\sin(a) & 0 \\ \sin(a) & \cos(a) & 0 \\ 0 & 0 & 1 \end{bmatrix} \qquad (2.4)$$

In this thesis, all rotation operations are taken to be rotating frame based, i.e., each subsequent rotation is performed about an axis that belongs to the preceding rotated frame.

Then, the transformation matrices $\hat{C}^{(e,w)}$ and $\hat{C}^{(w,b)}$ can be written as shown below.

$$\hat{C}^{(e,w)} = e^{\widetilde{u}_3 \eta_m} e^{-\widetilde{u}_2 \gamma_m} e^{\widetilde{u}_1 \varphi_m} \qquad (2.5)$$

$$\hat{C}^{(w,b)} = e^{\widetilde{u}_3 \beta} e^{-\widetilde{u}_2 \alpha} \qquad (2.6)$$

In Eq. (2.5), η_m, γ_m and φ_m are the azimuth, elevation, and bank angles of the wind frame with respect to the ENU frame. In Eq. (2.6), α is the angle of attack, β is the sideslip angle, and it is assumed that the body frame does not have any roll motion with respect to the wind frame.

In Figure 2.1 and Figure 2.2, α and β angles are shown to present relation between the body-fixed frame and the wind frame. The first step of transformation operation from body-fixed frame to wind frame is rotation about second basis vector of body-fixed frame. After the first step, the first basis vector of stability reference frame is obtained. The stability frame is significatory for the aforementioned transformation operation; nonetheless, it is not utilized in modeling work.

2.1.1.2 Kinematics

Consider an earth-fixed ENU (East-North-Up) frame, which is denoted with its origin and basis vectors as $\mathcal{F}_e = \mathcal{F}_e\left\{O;\ \vec{u}_1^{(e)}, \vec{u}_2^{(e)}, \vec{u}_3^{(e)}\right\}$. Then, the following velocity and acceleration equations are written for the missile by using the components of the velocity vector expressed in the wind frame $\mathcal{F}_w = \mathcal{F}_w\left\{C;\ \vec{u}_1^{(w)}, \vec{u}_2^{(w)}, \vec{u}_3^{(w)}\right\}$.

$$\vec{v} = V_m \vec{u}_1^{(w)} \Rightarrow$$

$$\bar{v}^{(w)} = V_m \bar{u}_1^{(w/w)} = V_m \bar{u}_1 \tag{2.7}$$

$$\bar{v}^{(e)} = V_m \bar{u}_1^{(w/e)} = V_m \hat{C}^{(e,w)} \bar{u}_1^{(w/w)} = V_m e^{\tilde{u}_3 \eta_m} e^{-\tilde{u}_2 \gamma_m} e^{\tilde{u}_1 \varphi_m} \bar{u}_1$$
$$= V_m e^{\tilde{u}_3 \eta_m} e^{-\tilde{u}_2 \gamma_m} \bar{u}_1 \Rightarrow$$

$$\bar{v}^{(e)} = V_m e^{\tilde{u}_3 \eta_m}(\bar{u}_1 cos\gamma_m + \bar{u}_3 sin\gamma_m)$$
$$= V_m(cos\eta_m cos\gamma_m \bar{u}_1 + sin\eta_m cos\gamma_m \bar{u}_2 + sin\gamma_m \bar{u}_3) \quad (2.8)$$

Note that

$$\bar{u}_1^{(w/e)} = \hat{C}^{(e,w)} \bar{u}_1^{(w/w)} = e^{\tilde{u}_3 \eta_m} e^{-\tilde{u}_2 \gamma_m} e^{\tilde{u}_1 \varphi_m} \bar{u}_1 = e^{\tilde{u}_3 \eta_m} e^{-\tilde{u}_2 \gamma_m} \bar{u}_1$$
$$= e^{\tilde{u}_3 \eta_m}(\bar{u}_1 \cos\gamma_m + \bar{u}_3 \sin\gamma_m)$$

$$\bar{u}_1^{(w/e)} = \bar{u}_1 cos\eta_m cos\gamma_m + \bar{u}_2 sin\eta_m cos\gamma_m + \bar{u}_3 sin\gamma_m \quad (2.9)$$

$$\bar{u}_2^{(w/e)} = \hat{C}^{(e,w)} \bar{u}_2^{(w/w)} = e^{\tilde{u}_3 \eta_m} e^{-\tilde{u}_2 \gamma_m} e^{\tilde{u}_1 \varphi_m} \bar{u}_2$$
$$= e^{\tilde{u}_3 \eta_m} e^{-\tilde{u}_2 \gamma_m}(\bar{u}_2 cos\varphi_m + \bar{u}_3 sin\varphi_m) \Rightarrow$$

$$\bar{u}_2^{(w/e)} = e^{\tilde{u}_3 \eta_m}(\bar{u}_2 cos\varphi_m + \bar{u}_3 sin\varphi_m cos\gamma_m - \bar{u}_1 sin\varphi_m sin\gamma_m)$$

$$\bar{u}_2^{(w/e)} = -\bar{u}_1(\sin\eta_m cos\varphi_m + \cos\eta_m \sin\gamma_m \sin\varphi_m) + \bar{u}_2(\cos\eta_m cos\varphi_m$$
$$- \sin\eta_m \sin\gamma_m \sin\varphi_m) + \bar{u}_3(\cos\gamma_m \sin\varphi_m) \quad (2.10)$$

$$\bar{u}_3^{(w/e)} = \hat{C}^{(e,w)} \bar{u}_3^{(w/w)} = e^{\tilde{u}_3 \eta_m} e^{-\tilde{u}_2 \gamma_m} e^{\tilde{u}_1 \varphi_m} \bar{u}_3$$
$$= e^{\tilde{u}_3 \eta_m} e^{-\tilde{u}_2 \gamma_m}(\bar{u}_3 cos\varphi_m - \bar{u}_2 sin\varphi_m) \Rightarrow$$

$$\bar{u}_3^{(w/e)} = e^{\tilde{u}_3 \eta_m}(\bar{u}_3 cos\varphi_m cos\gamma_m - \bar{u}_1 cos\varphi_m sin\gamma_m - \bar{u}_2 sin\varphi_m)$$

$$\bar{u}_3^{(w/e)} = \bar{u}_1(\sin\eta_m sin\varphi_m - \cos\eta_m \sin\gamma_m cos\varphi_m) - \bar{u}_2(\cos\eta_m sin\varphi_m$$
$$+ \sin\eta_m \sin\gamma_m cos\varphi_m) + \bar{u}_3(\cos\gamma_m cos\varphi_m) \quad (2.11)$$

The derivative of Eq. (2.8) leads to the following acceleration equations.

$$\bar{a}^{(e)} = \dot{\bar{v}}^{(e)} = \dot{V}_m e^{\tilde{u}_3\eta_m} e^{-\tilde{u}_2\gamma_m}\bar{u}_1 + V_m\dot{\eta}_m e^{\tilde{u}_3\eta_m}\tilde{u}_3 e^{-\tilde{u}_2\gamma_m}\bar{u}_1 - V_m\dot{\gamma}_m e^{\tilde{u}_3\eta_m} e^{-\tilde{u}_2\gamma_m}\tilde{u}_2\bar{u}_1 \Rightarrow$$

$$\bar{a}^{(e)} = \dot{V}_m e^{\tilde{u}_3\eta_m} e^{-\tilde{u}_2\gamma_m}\bar{u}_1 + V_m\dot{\eta}_m e^{\tilde{u}_3\eta_m} e^{-\tilde{u}_2\gamma_m} e^{\tilde{u}_2\gamma_m}\tilde{u}_3 e^{-\tilde{u}_2\gamma_m}\bar{u}_1 - V_m\dot{\gamma}_m e^{\tilde{u}_3\eta_m} e^{-\tilde{u}_2\gamma_m}\bar{u}_3 \Rightarrow$$

$$\bar{a}^{(e)} = e^{\tilde{u}_3\eta_m} e^{-\tilde{u}_2\gamma_m}[\dot{V}_m\bar{u}_1 + V_m\dot{\eta}_m e^{\tilde{u}_2\gamma_m}\tilde{u}_3 e^{-\tilde{u}_2\gamma_m}\bar{u}_1 + V_m\dot{\gamma}_m\bar{u}_3] \Rightarrow$$

$$\bar{a}^{(e)} = e^{\tilde{u}_3\eta_m} e^{-\tilde{u}_2\gamma_m}[\dot{V}_m\bar{u}_1 + (V_m\dot{\eta}_m cos\gamma_m)\bar{u}_2 + (V_m\dot{\gamma}_m)\bar{u}_3] \quad (2.12)$$

On the other hand, noting that $e^{\tilde{u}_1\varphi_m} e^{-\tilde{u}_1\varphi_m} = \hat{I}$ and $e^{\tilde{u}_3\eta_m} e^{-\tilde{u}_2\gamma_m} e^{\tilde{u}_1\varphi_m} = \hat{C}^{(e,w)}$, Eq. (2.12) can be manipulated further as follows.

$$\bar{a}^{(e)} = \left(e^{\tilde{u}_3\eta_m} e^{-\tilde{u}_2\gamma_m}\right)\left(e^{\tilde{u}_1\varphi_m} e^{-\tilde{u}_1\varphi_m}\right)[\dot{V}_m\bar{u}_1 + (V_m\dot{\eta}_m\cos\gamma_m)\bar{u}_2 + (V_m\dot{\gamma}_m)\bar{u}_3] \Rightarrow$$

$$\bar{a}^{(e)} = \hat{C}^{(e,w)} e^{-\tilde{u}_1\varphi_m}\left[\dot{V}_m\bar{u}_1 + (V_m\dot{\eta}_m\cos\gamma_m)\bar{u}_2 + (V_m\dot{\gamma}_m)\bar{u}_3\right] = \hat{C}^{(e,w)}\bar{a}^{(w)} \Rightarrow$$

$$\bar{a}^{(w)} = e^{-\tilde{u}_1\varphi_m}\left[\dot{V}_m\bar{u}_1 + (V_m\dot{\eta}_m\cos\gamma_m)\bar{u}_2 + (V_m\dot{\gamma}_m)\bar{u}_3\right] \Rightarrow$$

$$\bar{a}^{(w)} = \dot{V}_m\bar{u}_1 + \bar{u}_2 V_m(\dot{\gamma}_m sin\varphi_m + \dot{\eta}_m cos\gamma_m cos\varphi_m) + \bar{u}_3 V_m(\dot{\gamma}_m cos\varphi_m - \dot{\eta}_m cos\gamma_m sin\varphi_m) \quad (2.13)$$

2.1.1.3 Dynamics

According to the second law of Newton,

$$m\vec{a} = m\vec{g} + \vec{T} + \vec{F}_{AD} \quad (2.14)$$

Here, $\vec{g} = -g\vec{u}_3^{(e)}$ is the gravity vector, $\vec{T} = T\vec{u}_1^{(b)}$ is the thrust vector, $\vec{u}_1^{(b)}$ is the first basis vector of the body-fixed frame, and $\vec{F}_{AD} = -D\vec{u}_1^{(w)} + S\vec{u}_2^{(w)} + L\vec{u}_3^{(w)}$ is

the aerodynamic force expressed with the $drag\ (D)$, $side\ force\ (S)$ and $lift\ (L)$ components naturally in the wind frame.

The vector equation (2.14) can be expressed as the following matrix equation in the wind frame.

$$m\bar{a}^{(w)} = -mg\bar{u}_3^{(e/w)} + T\bar{u}_1^{(b/w)} - D\bar{u}_1 + S\bar{u}_2 + L\bar{u}_3 \Rightarrow$$

$$m\bar{a}^{(w)} = -mg\hat{C}^{(w,e)}\bar{u}_3^{(e/e)} + T\hat{C}^{(w,b)}\bar{u}_1^{(b/b)} - D\bar{u}_1 + S\bar{u}_2 + L\bar{u}_3 \qquad (2.15)$$

Note that, by taking transpose of Eq. (2.5) and recalling Eq. (2.6)

$$\hat{C}^{(w,e)} = \hat{C}^{(e,w)t} = \left(e^{\tilde{u}_3\eta_m}e^{-\tilde{u}_2\gamma_m}e^{\tilde{u}_1\varphi_m}\right)^t = e^{-\tilde{u}_1\varphi_m}e^{\tilde{u}_2\gamma_m}e^{-\tilde{u}_3\eta_m} \qquad (2.16)$$

$$\hat{C}^{(w,b)} = e^{\tilde{u}_3\beta}e^{-\tilde{u}_2\alpha} \qquad (2.17)$$

When Eqs. (2.13) and (2.15) are combined, they lead to the following equations.

$$\begin{aligned}
&m\dot{V}_m\bar{u}_1 + \bar{u}_2 mV_m(\dot{\gamma}_m sin\varphi_m + \dot{\eta}_m cos\gamma_m cos\varphi_m)\\
&+ \bar{u}_3 mV_m(\dot{\gamma}_m cos\varphi_m - \dot{\eta}_m cos\gamma_m sin\varphi_m)\\
&= -mge^{-\tilde{u}_1\varphi_m}e^{\tilde{u}_2\gamma_m}e^{-\tilde{u}_3\eta_m}\bar{u}_3^{(e/e)} + Te^{\tilde{u}_3\beta}e^{-\tilde{u}_2\alpha}\bar{u}_1^{(b/b)} - D\bar{u}_1\\
&+ S\bar{u}_2 + L\bar{u}_3 \Rightarrow
\end{aligned}$$

$$\begin{aligned}
&m\dot{V}_m\bar{u}_1 + \bar{u}_2 mV_m(\dot{\gamma}_m sin\varphi_m + \dot{\eta}_m cos\gamma_m cos\varphi_m)\\
&+ \bar{u}_3 mV_m(\dot{\gamma}_m cos\varphi_m - \dot{\eta}_m cos\gamma_m sin\varphi_m)\\
&= -mg(\bar{u}_3 cos\varphi_m cos\gamma_m + \bar{u}_2 cos\gamma_m sin\varphi_m + sin\gamma_m\bar{u}_1)\\
&+ T(\bar{u}_1 cos\alpha cos\beta + \bar{u}_2 cos\alpha sin\beta + \bar{u}_3 sin\alpha) - D\bar{u}_1\\
&+ S\bar{u}_2 + L\bar{u}_3
\end{aligned} \qquad (2.18)$$

Eq. (2.18) leads further to the following scalar equations.

$$m\dot{V}_m = Tcos\alpha cos\beta - D - mgsin\gamma_m \qquad (2.19)$$

$$mV_m(\dot{\gamma}_m sin\varphi_m + \dot{\eta}_m cos\gamma_m cos\varphi_m) = Tcos\alpha sin\beta + S - mgsin\varphi_m\, cos\gamma_m \quad (2.20)$$

$$mV_m(\dot{\gamma}_m cos\varphi_m - \dot{\eta}_m cos\gamma_m sin\varphi_m) = Tsin\alpha + L - mgcos\varphi_m\, cos\gamma_m \quad (2.21)$$

Furthermore, in the no-bank wind frame, i.e., the body frame and the wind frame do not have any roll motion with respect to each other, Eqs. (2.19) - (2.21) become

$$m\dot{V}_m = Tcos\alpha cos\beta - D - mgsin\gamma_m \quad (2.22)$$

$$mV_m\dot{\gamma}_m = T(cos\alpha sin\beta sin\varphi_m + sin\alpha cos\varphi_m) + Ssin\varphi_m + Lcos\varphi_m - mgcos\gamma_m \quad (2.23)$$

$$mV_m\dot{\eta}_m cos\gamma_m = T(cos\alpha sin\beta cos\varphi_m - sin\alpha sin\varphi_m) + Scos\varphi_m - Lsin\varphi_m \quad (2.24)$$

Suppose $\beta \cong 0$ as usual in a bank-to-turn motion. Then, $S \cong 0$, too. So, the above equations simplify to

$$m\dot{V}_m = Tcos\alpha - D - mgsin\gamma_m \quad (2.25)$$

$$mV_m\dot{\gamma}_m = T(sin\alpha cos\varphi_m) + Lcos\varphi_m - mgcos\gamma_m \quad (2.26)$$

$$mV_m\dot{\eta}_m cos\gamma_m = T(-sin\alpha sin\varphi_m) - Lsin\varphi_m \quad (2.27)$$

2.1.1.4 Bank-to-Turn Maneuver

Referring to Eqs. (2.25) – (2.27), the bank-to-turn maneuver can be accomplished by adjusting the lateral (azimuthal) acceleration $a_\eta = V_m\dot{\eta}_m cos\gamma_m$ and the elevational

acceleration $a_\gamma = V_m\dot{\gamma}_m$. These two accelerations can be adjusted by means of the bank angle φ_m and the lift force L.

In this maneuver, it is assumed that the thrust force T is specified as a function of time but it is not controllable. For example, it may almost be a constant. Thus, the speed V_m happens to be uncontrollable, too. Yet, its varying value can be estimated by integrating Eq. (2.25).

As for the necessary values of L and φ_m, they can be found from the following versions of Eqs. (2.26) and (2.27).

$$(L + Tsin\alpha)cos\varphi_m = m(a_\gamma + gcos\gamma_m) \tag{2.28}$$

$$(L + Tsin\alpha)sin\varphi_m = -ma_\eta \tag{2.29}$$

For the desired values of a_γ and a_η, Eqs. (2.28) and (2.29) give the necessary values of L and φ_m as follows.

$$L + Tsin\alpha = \sigma m\sqrt{\left(a_\gamma + gcos\gamma_m\right)^2 + a_\eta^2}\ ;\ \sigma = \pm 1 \tag{2.30}$$

$$\varphi_m = -atan2[\sigma a_\eta, \sigma\left(a_\gamma + gcos\gamma_m\right)] \tag{2.31}$$

However, the bank angle φ_m is supposed to be an *acute angle*. Therefore, σ must be such that

$$\sigma = sgn(a_\gamma + gcos\gamma_m) \tag{2.32}$$

Then, the bank angle formula becomes

$$\varphi_m = -atan2[\sigma a_\eta, \left|a_\gamma + gcos\gamma_m\right|] \tag{2.33}$$

On the other hand, assuming that α is small enough so that $sin\alpha \cong \alpha$, Eq. (2.30) can also be written as shown below by inserting that $L = L_\alpha \alpha + L_{\delta_e}\delta_e$

$$(L_\alpha + T)\alpha + L_{\delta_e}\delta_e = \sigma m\sqrt{\left(a_\gamma + gcos\gamma_m\right)^2 + a_\eta^2} \tag{2.34}$$

Here, L_α and L_{δ_e} are defined as follows.

$$L_\alpha = \frac{\partial L}{\partial \alpha} \tag{2.35}$$

$$L_{\delta_e} = \frac{\partial L}{\partial \delta_e} \tag{2.36}$$

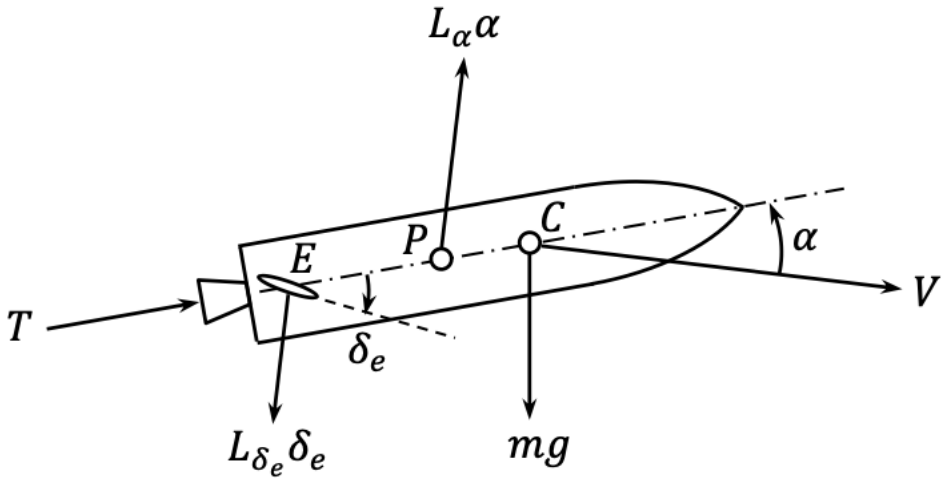


Figure 2.3 Side View of the Missile

Note that Eq. (2.34) contains two unknowns, which are α and δ_e. So, one more equation is required to find these unknowns. The second equation comes from the following pseudo static moment equation about the mass center C of the missile,

which is written assuming that the lift force consists of two parts, which are $L_\alpha \alpha$ that acts at the *pressure center P* and $L_{\delta_e}\delta_e$ that acts at the point E lying on the centerline of the missile and the common axis of the two elevator fins which are assumed to be acting in tandem as illustrated in Figure 2.3.

$$J_2\ddot{\theta} = [(L_{\delta_e}\delta_e)d_{CE} - (L_\alpha \alpha)d_{CP}]sin\alpha \cong 0 \tag{2.37}$$

θ is the pitch angle and obtained by using the $\theta = \alpha + \gamma_m$ relation [6].

It is assumed that the inertia moment $J_2\ddot{\theta} \cong 0$ in accordance with the approximate modeling of the missile as a particle. By using Eqs. (2.34) and (2.37), α and δ_e can be found as follows.

$$\alpha = \sigma m\sqrt{\left(a_\gamma + gcos\gamma_m\right)^2 + a_\eta^2} \,/\, [L_\alpha + \left(\frac{d_{CP}}{d_{CE}}\right)L_\alpha + T] \tag{2.38}$$

$$\delta_e = \left(\frac{d_{CP}}{d_{CE}}\right)(\frac{L_\alpha}{L_{\delta_e}})\alpha \tag{2.39}$$

2.1.1.5 Notes about the Angles

The *yaw-pitch-roll* angles (ψ, θ, ϕ) of the body frame, the *azimuth-elevation-bank* angles $(\eta_m, \gamma_m, \varphi_m)$ of the wind frame, and the aerodynamic angle (α, β) are related to each other according to the following rotational transformation equation.

$$\hat{C}^{(e,b)} = \hat{C}^{(e,w)}\hat{C}^{(w,b)} \tag{2.40}$$

Eq. (2.40) can also be written as follows by inserting the detailed expressions of the transformation matrices, paying attention to the fact that the earth frame is selected as ENU (East, North, Up) frame.

$$e^{\tilde{u}_3\psi}e^{-\tilde{u}_2\theta}e^{\tilde{u}_1\phi} = (e^{\tilde{u}_3\eta_m}e^{-\tilde{u}_2\gamma_m}e^{\tilde{u}_1\varphi_m})(e^{\tilde{u}_3\beta}e^{-\tilde{u}_2\alpha}) \tag{2.41}$$

Eq. (2.41) can be rearranged as

$$e^{\tilde{u}_3\beta}e^{-\tilde{u}_2\alpha} = e^{-\tilde{u}_1\varphi_m}e^{\tilde{u}_2\gamma_m}e^{\tilde{u}_3(\psi-\eta_m)}e^{-\tilde{u}_2\theta}e^{\tilde{u}_1\phi} \tag{2.42}$$

The angles α and β can be extracted from Eq. (2.42) as follows.

$$\bar{u}_3^t e^{\tilde{u}_3\beta}e^{-\tilde{u}_2\alpha}\bar{u}_1 = \bar{u}_3^t e^{-\tilde{u}_2\alpha}\bar{u}_1 = \bar{u}_3^t e^{-\tilde{u}_1\varphi_m}e^{\tilde{u}_2\gamma_m}e^{\tilde{u}_3(\psi-\eta_m)}e^{-\tilde{u}_2\theta}e^{\tilde{u}_1\phi}\bar{u}_1 \Rightarrow$$

$$sin\alpha = \bar{u}_3^t e^{-\tilde{u}_1\varphi_m}e^{\tilde{u}_2\gamma_m}e^{\tilde{u}_3(\psi-\eta_m)}e^{-\tilde{u}_2\theta}\bar{u}_1 \tag{2.43}$$

$$\bar{u}_1^t e^{\tilde{u}_3\beta}e^{-\tilde{u}_2\alpha}\bar{u}_2 = \bar{u}_1^t e^{\tilde{u}_3\beta}\bar{u}_2 = \bar{u}_1^t e^{-\tilde{u}_1\varphi_m}e^{\tilde{u}_2\gamma_m}e^{\tilde{u}_3(\psi-\eta_m)}e^{-\tilde{u}_2\theta}e^{\tilde{u}_1\phi}\bar{u}_2 \Rightarrow$$

$$sin\beta = -\bar{u}_1^t e^{\tilde{u}_2\gamma_m}e^{\tilde{u}_3(\psi-\eta_m)}e^{-\tilde{u}_2\theta}e^{\tilde{u}_1\phi}\bar{u}_2 \tag{2.44}$$

Meanwhile, Eq. (2.42) implies the following compatibility condition as well.

$$\bar{u}_3^t e^{-\tilde{u}_1\varphi_m}e^{\tilde{u}_2\gamma_m}e^{\tilde{u}_3(\psi-\eta_m)}e^{-\tilde{u}_2\theta}e^{\tilde{u}_1\phi}\bar{u}_2 = \bar{u}_3^t e^{\tilde{u}_3\beta}e^{-\tilde{u}_2\alpha}\bar{u}_2 = \bar{u}_3^t\bar{u}_2 = 0 \tag{2.45}$$

On the other hand, the aerodynamic angles are also related to the velocity components in the body and wind frames as indicated below.

$$\bar{v}^{(w)} = V_m\bar{u}_1^{(w/w)} = V_m\bar{u}_1 \tag{2.46}$$

$$\bar{v}^{(b)} = u\bar{u}_1^{(b/b)} - v\bar{u}_2^{(b/b)} - w\bar{u}_3^{(b/b)} = u\bar{u}_1 - v\bar{u}_2 - w\bar{u}_3 \tag{2.47}$$

Here, the second and third components appear with minus signs because the body frame is taken compatibly with the ENU version of the earth frame in such a way that the body frame becomes parallel to the earth frame when the body frame angles (ψ, θ, ϕ) happen to be zero. However, if the body frame were taken compatibly with the traditional NED (North, East, Down) version of the earth frame, then all components of $\bar{v}^{(b)}$ would appear with plus signs.

Note that

$$\bar{v}^{(b)} = \hat{C}^{(b,w)}\bar{v}^{(w)} \tag{2.48}$$

Hence,

$$u\bar{u}_1 - v\bar{u}_2 - w\bar{u}_3 = \left(e^{\tilde{u}_3\beta}e^{-\tilde{u}_2\alpha}\right)^t(V_m\bar{u}_1) = V_m e^{\tilde{u}_2\alpha}e^{-\tilde{u}_3\beta}\bar{u}_1 \Rightarrow$$

$$u\bar{u}_1 - v\bar{u}_2 - w\bar{u}_3 = V_m e^{\tilde{u}_2\alpha}(\bar{u}_1 cos\beta - \bar{u}_2 sin\beta)$$

$$= V_m(\bar{u}_1 cos\beta cos\alpha - \bar{u}_2 sin\beta - \bar{u}_1 cos\beta sin\alpha \Rightarrow$$

$$u = V_m cos\beta cos\alpha, v = V_m sin\beta, w = V_m cos\beta sin\alpha \tag{2.49}$$

Eq. Set (2.49) implies that

$$\beta = sin^{-1}(v/V_m) \tag{2.50}$$

$$\alpha = tan^{-1}(w/u) \tag{2.51}$$

$$V_m = \sqrt{u^2 + v^2 + w^2} \tag{2.52}$$

2.1.2 Thrust Model

Ramjet engines are jet engines that utilize the forward motion of the engine to compress incoming air, eliminating the need for a rotary compressor. Ramjets are highly suitable for applications that demand high speed and long-lasting propulsion,

particularly for Beyond Visual Range Air-to-Air Missiles (BVRAAM), thanks to their exceptional speed capabilities.

For ramjet engines to function optimally, several criteria, including a minimum speed, must be met. Below this threshold velocity, they are unable to generate the necessary compression for efficient combustion. Ramjets typically have a top limit of operational speed that reaches high supersonic and hypersonic velocities, typically about Mach 6. Violating this speed limit can result in material and combustion issues due to the increased temperature of the incoming air. Furthermore, the angle of attack is restricted to prevent the ramjet engine from encountering choking, a condition characterized by the inability to acquire an adequate amount of air.

In order to surpass the constraints of ramjets and sustain the optimal performance of the missile for its entire cruising period, a two-stage propulsion system is typically employed.

Phase One: Solid Rocket Booster

Prior to attaining the necessary operational velocity, solid rocket propellant is employed in the ramjet. This thruster generates the initial propulsion needed to accelerate the missile to a velocity at which the ramjet can be activated. The thruster functions briefly, often for a few seconds, generating a substantial amount of propulsion to rapidly attain the desired velocity.

Phase Two: Ramjet Propulsion System

When the missile's speed hits around Mach 2, the ramjet engine becomes operational. At this point, the solid rocket propellant is either discharged or depleted, and the ramjet acquires control. The ramjet engine sustains the missile's trajectory and delivers extended-duration and extended-range propulsion. This provides enhanced propulsion by utilizing solid rocket motors in addition to other more efficient methods [18].

Thrust force can be calculated for both stages by using the following equation.

$$T = I_{sp} g \dot{m} \tag{2.53}$$

$$t_{booster} = \frac{m_{booster}}{\dot{m}_{booster}} = \frac{m_{booster}}{(\frac{T_{booster}}{I_{sp_{booster}} g})} \tag{2.54}$$

$$t_{ramjet} = \frac{m_{ramjet}}{\dot{m}_{ramjet}} = \frac{m_{ramjet}}{(\frac{T_{ramjet}}{I_{sp_{ramjet}} g})} \tag{2.55}$$

Eqs. 2.54 and 2.55 are derived by using the fact that rate of change of fuel mass is equal to the ratio of consumed fuel mass to duration of propulsion. Then, it is combined with the $\dot{m}$ expression from Eq. 2.53.

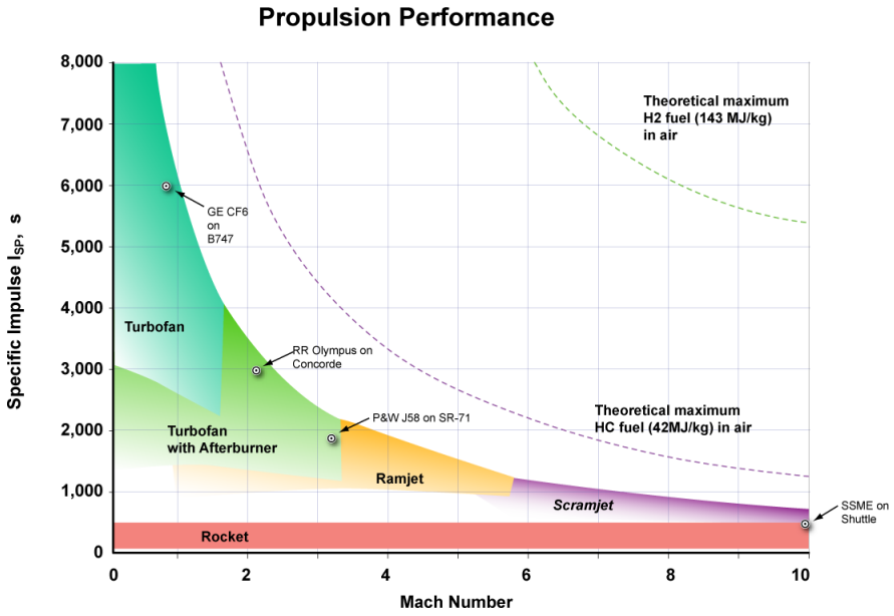


Figure 2.4 Specific Impulse of Various Jet Engines [19]

Specific impulse - I_{sp} is defined as the thrust generated per unit weight flow of the fuel. It is a crucial performance metric for propulsion systems. The quantitative assessment of a rocket or jet engine's efficiency is determined by establishing a relationship between the thrust generated and the rate at which fuel is used.

Ramjet engines are designed to operate efficiently at high speeds, making specific impulse a critical factor in assessing their efficiency. A higher specific impulse provides that the missile can achieve higher velocities or longer ranges using the same amount of fuel.

If $t_{sim} \leq t_{booster}$ which represents the booster phase of thrust model,

$$T_{booster} = 35\ kN, I_{sp_{booster}} = 300\ s, m_{booster} = 45\ kg \tag{2.56}$$

If $t_{booster} \leq t_{sim} \leq t_{ramjet}$ where the ramjet engine is active,

$$T_{ramjet} = 7.5\ kN, I_{sp_{ramjet}} = 1000\ s, m_{ramjet} = 15\ kg \tag{2.57}$$

2.1.3 Aerodynamical Model of the Missile

Table 2.1 Physical Parameters of the Missile

Parameter	Value	Unit (SI)
m	185	kg
m_{fuel}	60	kg
m_{empty}	125	kg
J_1	$\frac{0.9218m}{125}$	$kg\ m^2$
J_2	$\frac{136.4223m}{125}$	$kg\ m^2$
J_3	$\frac{136.4223m}{125}$	$kg\ m^2$
L_{Ref}	0.178	m
d_{CP}	1.9	m
d_{CE}	3.7	m

For the given missile configuration, Missile DATCOM [20] is used to obtain aerodynamical database including coefficients for aerodynamical forces and moments. The physical parameters included in Table 2.1 serve as inputs for the Missile DATCOM tool. These parameters are utilized to approximate a real BVRAAM system and simulate its aerodynamic characteristics.

$$C_i = C_i(M, \alpha, \beta, \delta_a, \delta_e, \delta_r) \tag{2.58}$$

The database has lookup tables with aerodynamic moment and force coefficients. The force and moment coefficients are determined by generating lookup tables using the Mach number, angle of attack, angle of sideslip, elevator fin deflection (δ_e), aileron fin deflection (δ_a), and rudder fin deflection (δ_r).

The missile is presumed to fly in an X configuration, hence the aerodynamic data is gathered for the wings and fins positioned at angles of *45°, 135°, 225°, and 315°*. The flight regime area is defined in Missile DATCOM using the flight parameters as

$$\alpha = \{-30, -25, -20, -15, -12, -10, -8, -6, -4, -2, 0, 2, 4, 6, 8, 10, 12, 15, 20, 25, 30\}°$$

$$\beta = \{-10, -5, 0, 5, 10\}°$$

$$M = \{0.8, 0.9, 0.95, 1, 1.05, 1.1, 1.2, 1.5, 2, 2.5, 3, 3.5, 4\}\ Mach$$

The aerodynamical reference area and dynamic pressure are calculated as

$$S_{Ref} = \frac{\pi}{4} d^2 = \frac{\pi}{4} L_{Ref}^2 \tag{2.59}$$

$$Q_d = \frac{1}{2} \rho V_m^2 \tag{2.60}$$

While computing the dynamic pressure at a specific height, the ICAO formula [21] is used for the ambient air density ρ. That is,

$$\rho = \begin{cases} \rho_0 (1 - 0.00002256h)^{4.256}\ for\ h \leq 10000\ m \\ 0.412 e^{-0.000151(h-10000)} for\ h > 10000\ m \end{cases} \tag{2.61}$$

In this formula, $\rho_0 = 1.223\ kg/m^3$ is the air density at the sea level and h is the altitude above the sea level.

The Mach number is also obtained by using the ICAO formulation as shown below

$$M = \frac{V_m}{C_S} \tag{2.62}$$

C_S is the speed of sound and obtained as

$$C_S = \gamma R \tau \tag{2.63}$$

γ is the specific heat ratio of air and taken as 1.4, R is the universal air gas constant being equal to $287\ J/kgK$ and τ is the temperature. τ_0 is $288.15\ K$.

$$\tau = \begin{Bmatrix} \tau_0(1 - 0.00002256h)\ for\ h \leq 10000\ m \\ 0.7744\tau_0\ for\ h > 10000\ m \end{Bmatrix} \tag{2.64}$$

Moreover, the lift force produced from Eq. (2.30) is utilized to compute drag.

Aspect ratio and other features of the missile are often used to predict aerodynamic efficiency because the lift-to-drag increases with aspect ratio, improving the fuel economy.

$$AR = \frac{length\ of\ missile\ (L)}{diameter\ of\ missile\ (d)} = \frac{3.7}{0.178} \approx 20.79 \tag{2.65}$$

The performance of aspect ratio (AR) related to the lift-to-drag-ratio is illustrated in the formula used to calculate the drag coefficient of a missile.

$$C_D = C_{D,0} + \frac{C_L^2}{(AR)(e)(\pi)} \tag{2.66}$$

$C_{D,0} \approx 0.5$ is taken as an average value for all the flight conditions and it is the zero-lift drag coefficient. The Oswald efficiency (e) is a coefficient that quantifies the change in drag with lift of a three-dimensional wing, in comparison to an ideal wing with the same aspect ratio and an elliptical lift distribution. It is taken as 0.6.

$$D = Q_d S_{Ref} C_D \tag{2.67}$$

2.1.3.1 Notes about Elevator Deflection and Angle of Attack

As explained by Eqs. (2.38) and (2.39), $L_\alpha \; and \; L_{\delta_e}$ are required to obtain $\alpha \; and \; \delta_e$.

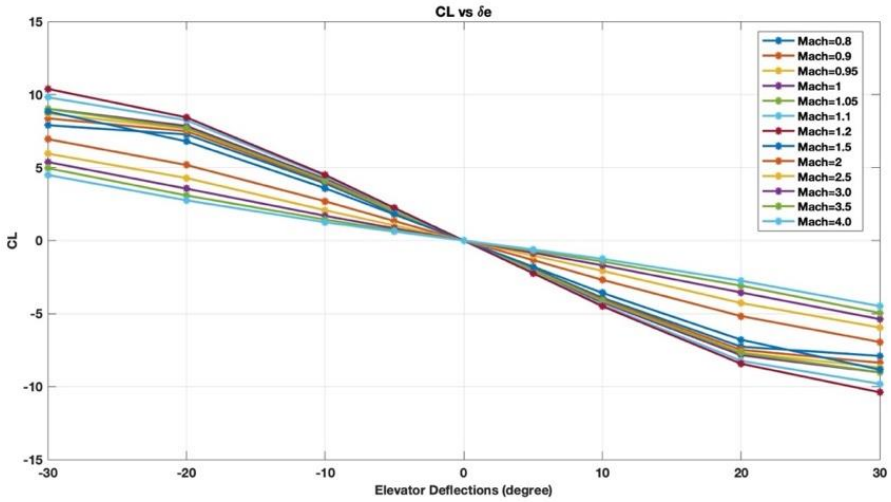


Figure 2.5 Control Derivative of Lift Force Coefficient vs Elevator Deflections

Note that, the lift force coefficient versus elevator deflections is plotted for the case of zero angle of attack. ($\alpha = 0°$)

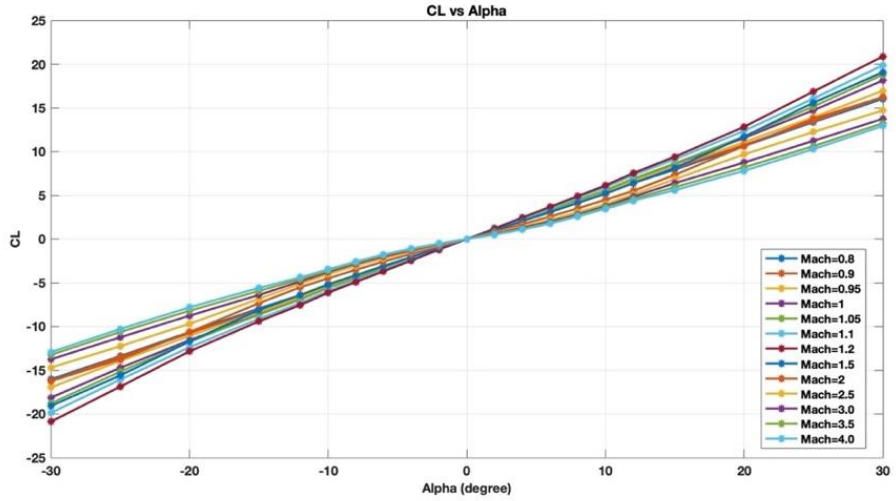


Figure 2.6 AoA Stability Derivative of Lift Force Coefficient vs AoA

Since the trends of lines are almost linear in both figures given above, average slope values for $C_{L_{\delta_e}}$ and C_{L_α} are calculated. Then, 5th order polynomial curve fitting via MATLAB Curve Fitting Toolbox [22] for $C_{L_{\delta_e}}$ and C_{L_α} values are performed. After fitting operation, $C_{L_{\delta_e}}$ and C_{L_α} depend on only Mach number - $C_{L_{\delta_e}}(M)\ and\ C_{L_\alpha}(M)$.

$$C_{L_{\delta_e}}(M) = -1.11M^5 + 14.69M^4 - 74.6M^3 + 178.4M^2 - 191.3M + 51.16 \quad (2.68)$$

$$C_{L_{\delta_e}}(M) = 1.089M^5 - 15.6M^4 + 86.18M^3 - 226M^2 + 271.4M - 81.78 \quad (2.69)$$

$$L_{\delta_e} = qS_{Ref}C_{L_{\delta_e}} \quad (2.70)$$

$$L_\alpha = qS_{Ref}C_{L_\alpha} \quad (2.71)$$

$$L = L_{\delta_e} + L_\alpha \quad (2.72)$$

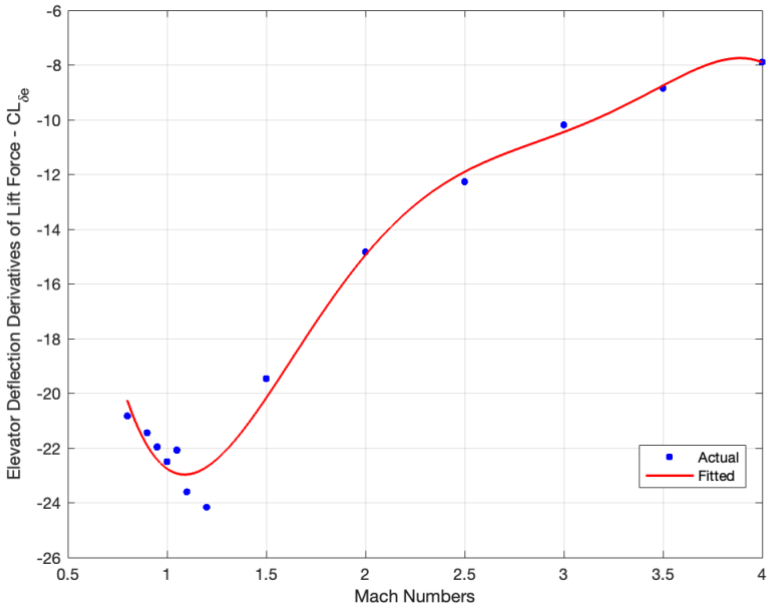


Figure 2.7 Actual and Fitted $C_{L_{\delta_e}}$ vs Mach Number

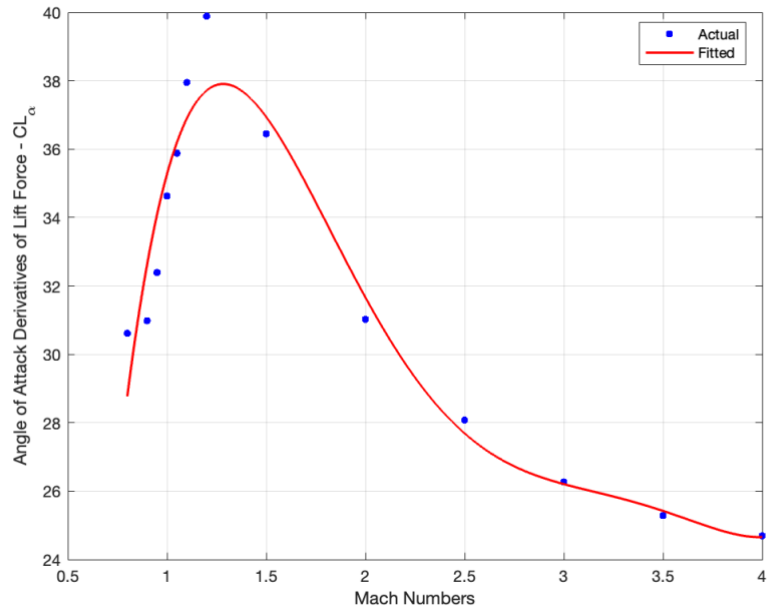


Figure 2.8 Actual and Fitted $C_{L_{\alpha}}$ vs Mach Number

2.1.4 Roll Autopilot

To obtain the aileron deflection command ($\delta_{a,c}$), a roll position autopilot is employed. The roll position autopilot is usually designed with an inner angular velocity (p) loop and an outer angular position (ϕ) loop. Missiles utilize the roll autopilot to counteract any roll deviations that may occur due to aerodynamic cross coupling, while independently moving in the pitch and yaw planes. It is shown as a block diagram in Figure 2.9. The inner rate loop enhances the damping effect, i.e., provides stability augmentation, while the outer position loop achieves the roll command tracking. As illustrated in Figure 2.9, the missile's inertial navigation system (INS) provides feedback on the roll angular position and angular velocity.

As mentioned in 2.1.1.1, since the body frame does not have any roll motion with respect to the wind frame, the roll command is taken as $\phi_c = \varphi_m$.

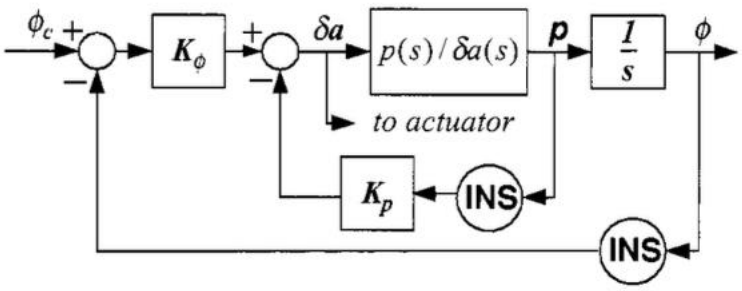


Figure 2.9 Roll Rate and Position Feedback Loops [23]

The roll moment damping derivative is

$$M_{lp} = \frac{Q_d S_{Ref} L_{Ref}^2 C_{l_p}(M, \alpha)}{2V_m J_1} \tag{2.73}$$

The roll moment control derivative is

$$M_{l\delta_a} = \frac{Q_d S_{Ref} L_{Ref} \; C_{l_{\delta_a}}(M, \alpha)}{J_1} \tag{2.74}$$

The transfer function between the roll rate and the aileron angle is

$$\frac{p(s)}{\delta_a(s)} = \frac{M_{l\delta_a}}{s - M_{lp}} \tag{2.75}$$

Pole placement method is used to design the autopilot with the flexibility of establishing natural frequency and damping. Natural frequency and damping ratio of roll autopilot are designated as

$$\omega_{n,roll} \cong 126\ rad/s\ (20\ Hz),$$
$$\zeta_{roll} = 0.707 \tag{2.76}$$

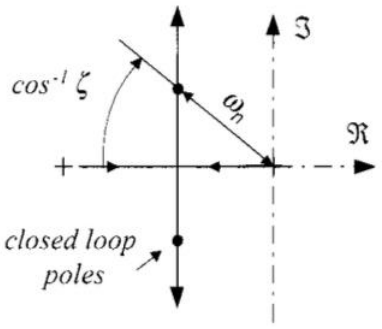


Figure 2.10 Root Locus Diagram of Roll Autopilot [23]

Closed loop poles shown in Figure 2.10 are obtained as

$$s_{1,2} = -\sigma \pm j\omega_d \tag{2.77}$$

$$\sigma = \zeta\omega_n \tag{2.78}$$

$$\omega_d = \omega_n\sqrt{1-\zeta^2} \tag{2.79}$$

Then, the closed loop transfer function becomes

$$\frac{\phi(s)}{\phi_c(s)} = \frac{K_\phi M_{l\delta_a}}{s^2 + (K_p M_{l\delta_a} - M_{lp})s + K_\phi M_{l\delta_a}} = \frac{K_\phi M_{l\delta_a}}{s^2 + 2\zeta\omega_n s + \omega_n^2} \tag{2.80}$$

$$K_\phi = \frac{\omega_n^2}{M_{l\delta_a}} \tag{2.81}$$

$$K_p = \frac{2\zeta\omega_n + M_{lp}}{M_{l\delta_a}} \tag{2.82}$$

By considering the CAS, the transfer functions involving the roll command, the bank angle, and the aileron deflection command are written as follows.

$$\frac{\delta_{a,c}(s)}{\phi_c(s)} = \frac{K_\phi s(s - M_{lp})}{s^2 + (K_p M_{l\delta_a} - M_{lp})s + K_\phi M_{l\delta_a}} = \frac{K_\phi s(s - M_{lp})}{s^2 + 2\zeta\omega_n s + \omega_n^2} \tag{2.83}$$

For a second order system represented by the transfer function of roll position autopilot in Eq. 2.80, transient response specifications for maximum (percent) overshoot, M_p, settling time (with 2% criterion) T_s, and rise time T_r are calculated as [24]

$$M_p = e^{-\left(\frac{\zeta}{\sqrt{1-\zeta^2}}\right)\pi} \tag{2.84}$$

$$T_s = \frac{4}{\zeta \omega_n} \tag{2.85}$$

$$T_r = \frac{\pi - \beta}{\omega_d} \tag{2.86}$$

As an example, the resultant design metrics of $\alpha = 5°, \beta \cong 0°, M = 3\ Mach\ and\ h_m = 6\ km$ are presented in the table given below.

Table 2.2 Roll Position Autopilot Metrics

GM (dB)	**PM (deg)**	**Rise Time (s)**	**Settling Time (s)**	**Overshoot (%)**
Inf	65.5246	0.0139	0.0233	4.3251

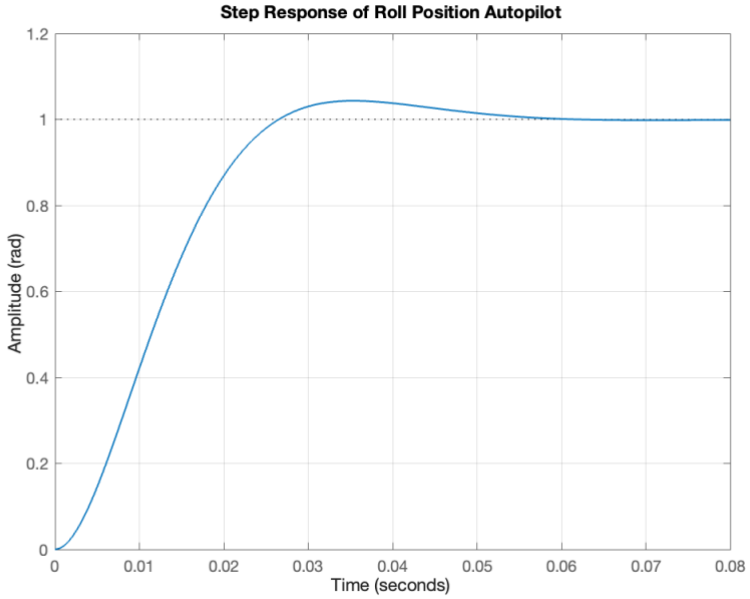


Figure 2.11 Step Response of the Roll Autopilot

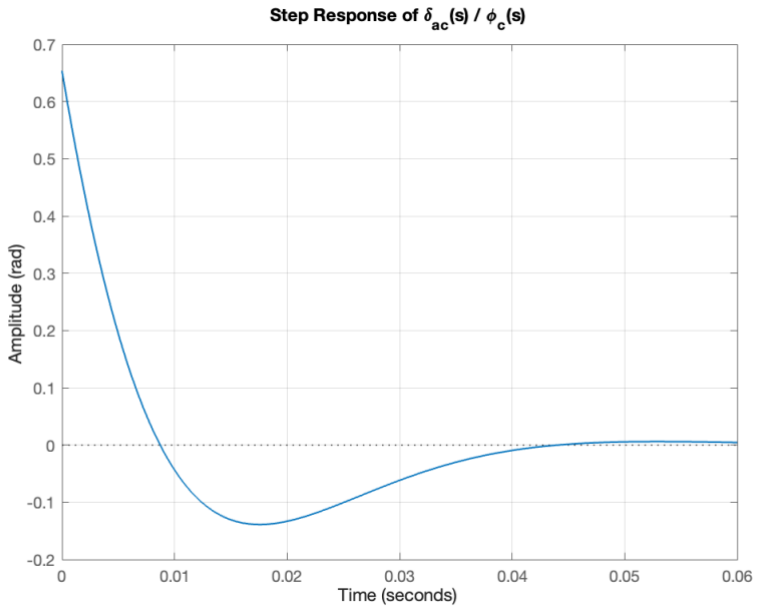


Figure 2.12 Step Response of the Aileron Deflection Command

2.1.5 Control Actuation System

Control actuation system is basically a motor system that actuates fins. It has its own closed loop control mechanism which takes autopilot fin commands as input and reacts on the system with its output according to its command tracking performance.

The second order CAS has $\omega_{n,CAS} \cong 377\, rad/s$ $(60\, Hz)$ and $\zeta_{CAS} = 0.707$ as natural frequency and damping ratio, respectively.

$$\frac{\delta(s)}{\delta_c(s)} = \frac{\omega_{n,CAS}^2}{s^2 + 2\zeta_{CAS}\omega_{n,CAS}s + \omega_{n,CAS}^2} \tag{2.87}$$

Also, CAS is accepted to provide maximum $30°$ of control surface deflections with maximum $300°/s$ turn rates.

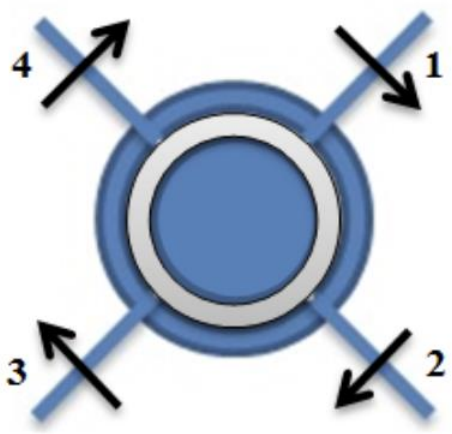


Figure 2.13 X Configuration of Fins [25]

When viewed from a rear perspective, the deflection angles that result in a positive roll motion are indicated by arrows pointing in the direction of positive deflection angles. To alter the missile's path towards the right or left, all four control surfaces deflect at an identical angle. Pitch refers to the change of the missile's angle of descent or ascent. If the deflections of 1 and 2 are positive (+) and the deflections of 3 and 4 are negative (-), then the missile is performing a pitch-up maneuver. When the missile shows deflections in the other direction, it indicates a pitch-down motion. Yaw is the term used to describe the rotational motion of a projectile. When the numbers 1 and 4 exhibit negative deflections and the numbers 2 and 3 exhibit positive deflections, the missile will turn right when viewed from behind. If the missile encounters deflections in the opposite direction, it will veer towards the left.

These four fins collectively induce three rotational movements along each body axis.

$$\delta_a = aileron\ deflection - induce\ roll\ motion$$

$$\delta_e = elevator\ deflection - induce\ pitch\ motion$$

$$\delta_r = rudder\ deflection - induce\ yaw\ motion$$

The following Eq. 2.88 presents a prevalent fin allocation for the X configuration [25].

$$\begin{aligned} \delta_1 &= \delta_a + \delta_e + \delta_r \\ \delta_2 &= \delta_a + \delta_e - \delta_r \\ \delta_3 &= \delta_a - \delta_e - \delta_r \\ \delta_4 &= \delta_a - \delta_e + \delta_r \end{aligned} \tag{2.88}$$

Since BTT (Bank-to-Turn) flight principle is used, $\delta_r \cong 0$.

2.2 Mathematical Model of the Target

Kinematic model of the target is used for simulation studies. As mentioned in Chapter 1, the modeling of the target is not in the scope of this thesis. It is assumed that the data such as the target's precise coordinates, velocity and heading can be transmitted to the missile accurately in a consistent and uninterrupted manner from a ground station during the midcourse phase. During the terminal phase with PNG, the missile uses its own facilities, such as IMU and seeker.

The following equations describe the kinematic model of the target to simulate its motion.

$$\frac{dV_t}{dt} = a_{x,t} \tag{2.89}$$

$$\frac{d\eta_t}{dt} = \frac{a_{y,t}}{V_t cos\gamma_t} \tag{2.90}$$

$$\frac{d\gamma_t}{dt} = \frac{a_{z,t}}{V_t} \tag{2.91}$$

$$\frac{dx_t}{dt} = V_t cos\gamma_t cos\eta_t \tag{2.92}$$

$$\frac{dy_t}{dt} = V_t cos\gamma_t sin\eta_t \tag{2.93}$$

$$\frac{dz_t}{dt} = V_t sin\gamma_t \tag{2.94}$$

CHAPTER 3

GUIDANCE METHODS

Chapter 3 explains the guidance methods used in this study in a detailed way. The distinctions between the missile's midcourse and terminal guidance phases are also covered. Following this, the proposed hybrid guidance, which comprises an optimal midcourse phase and terminal phase with PN guidance, is presented. In order to evaluate performance of the proposed method, a reference guidance law that is designated as "PN Guidance with Lofting" [12] is introduced and applied throughout the missile-target engagement for the sake of comparison.

Missile guidance can be categorized into two primary stages: midcourse guidance and terminal guidance. During the midcourse phase, which takes place after the launch and before the terminal phase begins, the primary objective is to effectively minimize the time to reach the entry of terminal phase. Transition from midcourse to terminal phase can be defined as entering a sphere with a specified radius. The radius is specified as the range of terminal guidance phase. Therefore, the final distance at the end of the midcourse phase is fixed as the specified radius of the entry sphere. Optimality can be defined as either the shortest possible flying time or the highest achievable terminal kinetic energy or both. As a matter of fact, the minimized reaching time implies maximized terminal kinetic energy. The terminal phase denotes the concluding segment of the flight, whereby the target's movements exert a substantial influence on the missile's acceleration requirements. Hence, it is beneficial for the missile to preserve as much kinetic energy as possible following the midcourse phase.

The proposed hybrid guidance law treats the midcourse phase as an optimal control problem. During the terminal phase, where the range between the missile and the

target is less than 10 km, PN guidance is used to ensure that the target is successfully hit, even if it tries to evade detection or avoid being hit.

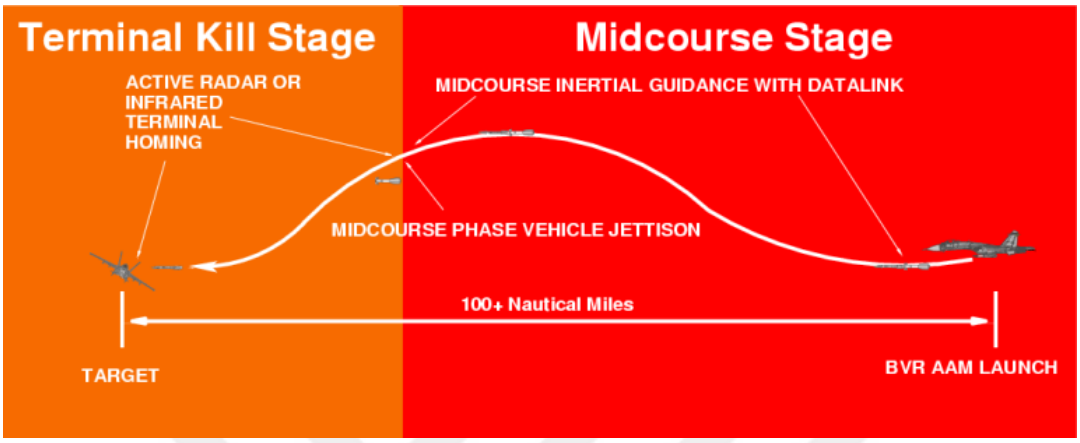


Figure 3.1 Typical Guidance Phases of a BVRAAM [31]

3.1 Optimal Midcourse Guidance

Optimal midcourse guidance refers to the process of trajectory optimization, which involves solving an optimal control problem. The problem is solved through nonlinear programming via direct collocation method. Direct collocation approaches convert a continuous-time trajectory optimization issue into a nonlinear program. A nonlinear program is a restricted parameter optimization problem that has nonlinear components in either its objective or constraint function. A trajectory that meets the system dynamics, boundary requirements and constraints is considered feasible, and the related controls are deemed admissible. An optimal trajectory is defined as one that reduces an objective function while remaining feasible.

3.1.1 Definitions of Optimal Control Problem

A viable solution to a trajectory optimization problem is one that satisfies all the restrictions of the problem. An objective function is used to mathematically describe the idea of the "optimal" route.

System dynamics remains continuous throughout the entire trajectory optimization process. It is used as a nonlinear equality constraint.

An objective function typically comprises two parts: a boundary objective indicated as $J(*)$ and an alternative integral that spans the entire trajectory, with the integrand represented by $w(*)$. A problem that includes both components is known as being in Bolza form. A problem with only the integral component is in Lagrange form, whereas a problem with only a boundary component is in Mayer form. In this study, an objective function in the Bolza form is used to be minimized. That is,

$$\min_{t_0,t_F,x(t),u(t),} \left\{ J_b\big(t_0,t_F,x(t_0),x(t_F)\big) + \int_{t_0}^{t_F} w(\tau\,,x(\tau),u(\tau))d\tau \right\} \quad \Rightarrow$$

$$\min_{t_0,t_F,x(t),u(t),} \left\{ \mu_\lambda|\lambda_z| + \mu_\lambda|\lambda_y| + \int_{t_0}^{t_F} d\tau \right\}$$

Here, λ_z and λ_y are the line-of-sight angles in the vertical pitch and horizontal yaw planes. As for μ_λ, it is a suitably selected weighting coefficient. As mentioned before, the magnitudes of these angles are also required to be minimized as the missile enters the spherical manifold of the terminal guidance phase. However, if the missile enters the manifold with sufficiently high kinetic energy, then this requirement may be relaxed by taking $\mu_\lambda = 0$.

On the other hand, by taking $t_0 = 0$, the optimization process can also be expressed simply in the Mayer form. That is,

$$\min_{t_0, t_F, x(t), u(t),} \{\mu_\lambda |\lambda_z| + \mu_\lambda |\lambda_y| + t_F\} \tag{3.1}$$

Within optimization, "decision variables" are the variables arranged to reduce the objective function. The decision variables usually consist of the final time (t_F), along with the state trajectory $x(t)$ and control trajectory $u(t)$.

System dynamics:

$$\dot{x} = f\big(t, x(t), u(t)\big) \tag{3.2}$$

Boundary constraints:

$$g\big(t_0, t_F, x(t_0), x(t_F)\big) \leq 0 \tag{3.3}$$

Path constraints:

$$h(t, x(t), u(t)) \leq 0 \tag{3.4}$$

Lower and upper bounds described for the state variables, control inputs, and terminal times:

$$\begin{aligned} x_{low} \leq x(t) \ll x_{upp} \\ u_{low} \leq u(t) \ll u_{upp} \\ t_{low} \leq t_0 < t_F \ll t_{upp} \end{aligned} \tag{3.5}$$

3.1.2 Direct Collocation Method

A direct collocation method discretizes the trajectory optimization problem by transforming it into a problem of nonlinear programming.

Firstly, discretization is applied to a continuous trajectory optimization problem by approximating all continuous functions in the problem formulation as polynomial splines. A spline is a mathematical function composed of a series of polynomial segments. Polynomials are utilized due to their facilitating key characteristics, i.e., they may be expressed by a limited set of coefficients, and it is simple to calculate integrals and derivatives of polynomials based on these coefficients.

A nonlinear programming problem is a restricted parameter optimization problem that has nonlinear components in either its objective or constraint function or both, which can be expressed generically as shown below. In the expression provided below, the argument z represents the decision variables including the state variables, control inputs and final time.

$$\min_{z} J(z)$$

subject to

$$f(z) = 0$$

$$g(z) \leq 0$$

$$z_{low} \leq z \leq z_{upp}$$

A trajectory that meets the system dynamics, boundary requirements and constraints is considered feasible, and the related controls are deemed admissible. An optimal trajectory is defined as one that reduces an objective function while remaining feasible.

3.1.3 Trapezoidal Discretization

The continuous system dynamics must be transformed into a collection of constraints that can be enforced on the current state and managed at the collocation points. This is the application of trapezoid quadrature, sometimes referred to as the trapezoid rule. The main concept is that the transition in status from two nearby places is equivalent to the integration of the system's dynamics. The integral is approximated using trapezoidal quadrature, where h_k is defined as $t_{k+1} - t_k$.

In other words, the direct collocation approach describes system dynamics as a collection of limitations called collocation constraints. Trapezoidal collocation involves constructing collocation constraints by expressing the dynamics in integral form and then approximating the integral using trapezoidal quadrature. The relevant equations are as written below.

$$\dot{x} = f \tag{3.6}$$

$$\int_{t_k}^{t_{k+1}} \dot{x} dt = \int_{t_k}^{t_{k+1}} f dt \tag{3.7}$$

$$x_{k+1} - x_k \approx \frac{h_k}{2}[f_{k+1} + f_k] \approx \frac{h_k}{2}[\dot{x}_{k+1} + \dot{x}_k] \tag{3.8}$$

A system of equations is derived which provides an approximation of the dynamics occurring between every pair of collocation locations. The constraints are referred to as collocation constraints and the associated constraint equations are enforced as expressed below in every segment of the trajectory, i.e., for $k = 0, \dots, (N-1)$.

$$
\begin{aligned}
x_{m_{k+1}} - x_{m_k} &= \frac{h_k}{2}\left[\dot{x}_{m_{k+1}} + \dot{x}_{m_k}\right] \\
y_{m_{k+1}} - y_{m_k} &= \frac{h_k}{2}\left[\dot{y}_{m_{k+1}} + \dot{y}_{m_k}\right] \\
z_{m_{k+1}} - z_{m_k} &= \frac{h_k}{2}\left[\dot{z}_{m_{k+1}} + \dot{z}_{m_k}\right] \\
V_{m_{k+1}} - V_{m_k} &= \frac{h_k}{2}\left[\dot{V}_{m_{k+1}} + \dot{V}_{m_k}\right] \\
\gamma_{m_{k+1}} - \gamma_{m_k} &= \frac{h_k}{2}\left[\dot{\gamma}_{m_{k+1}} + \dot{\gamma}_{m_k}\right] \\
\eta_{m_{k+1}} - \eta_{m_k} &= \frac{h_k}{2}\left[\dot{\eta}_{m_{k+1}} + \dot{\eta}_{m_k}\right]
\end{aligned}
\tag{3.9}
$$

3.1.4 Constraints

Aside from the collocation constraints that govern/enforce the system dynamics, there may also be restrictions on the state and control variables, path constraints, and boundary constraints. These constraints are all handled by enforcing them at specific collocation points. For example, simple limits on the state and control variables are approximated as follows.

$$
\begin{aligned}
x < 0 \ &\rightarrow x_k < 0 \quad \forall k, \\
u < 0 \ &\rightarrow u_k < 0 \quad \forall k, \\
g\left(t_0, t_F, x(t_0), x(t_F)\right) < 0 \ &\rightarrow x_k < 0 \quad \forall k, \\
h(t, x(t), u(t)) < 0 \ &\rightarrow x_k < 0 \quad \forall k,
\end{aligned}
\tag{3.10}
$$

3.1.5 Interpolation

Trapezoidal collocation approximates the control trajectory and system dynamics as piecewise linear functions, referred to as linear splines, as represented in Figure 3.2 and Figure 3.4. In spline construction, a knot point refers to a location that connects two polynomial segments. In trapezoidal collocation, the spline's knot points overlap with the collocation points.

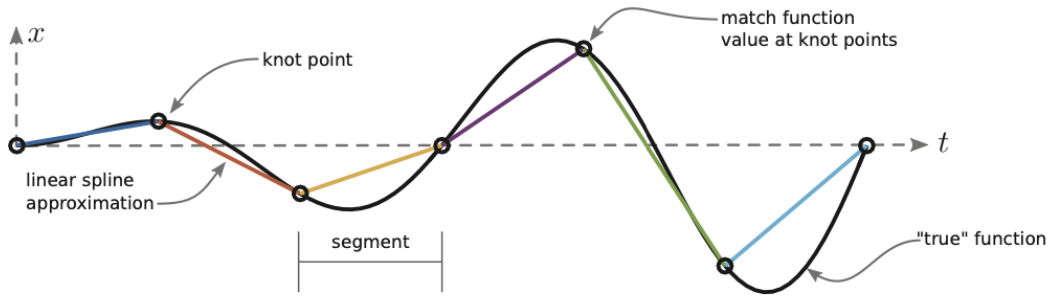


Figure 3.2 Function Approximation Using a Linear Spline [26]

Beginning by creating the control trajectory, which will be a basic linear spline. Given the time and control values at each knot point, it is straightforward to calculate the formula for u inside the interval $[t_k, t_{k+1}]$. In order to maintain readability in the mathematical context, it is established that Δ_k as $t - t_k$, and h_k as the difference between t_{k+1} and t_k.

$$u(t) \approx u_k + \frac{\Delta_k}{h_k}(u_{k+1} - u_k) \tag{3.11}$$

The state trajectory is represented by using a quadratic spline, which is a segmented quadratic function.

The trapezoidal collocation equations are exact when the system dynamics vary linearly between any two knot points, a fact that we use to approximate the dynamics over a single segment, i.e., for $t \in [t_k, t_{k+1}]$, as shown below:

$$f(t) = \dot{x}(t) \approx f_k + \frac{\Delta_k}{h_k}(f_{k+1} - f_k) \tag{3.12}$$

Since x is of interest rather than $\dot{x}$, a quadratic expression for the state is obtained by integrating both sides of Equation (3.12).

$$x(t) = \int \dot{x}dt \approx c + f_k\Delta_k + \frac{\Delta_k^2}{2h_k}(f_{k+1} - f_k) \tag{3.13}$$

Figure 3.3 presents how a linear control segment and quadratic state segment are constructed. Spline equations are specifically utilized for trapezoidal collocation due to a direct relationship between the collocation equations and the interpolating spline. If the control is a spline of order n, then the state is represented by a spline of order $n + 1$.

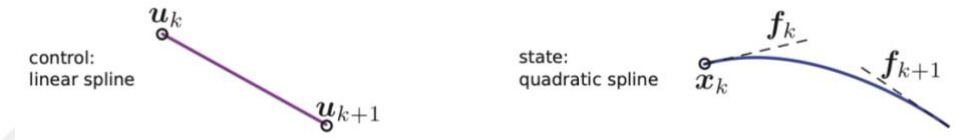


Figure 3.3 Illustration of the Linear and Quadratic Spline Segments [26] (that are used to approximate the control and state trajectories for trapezoidal collocation)

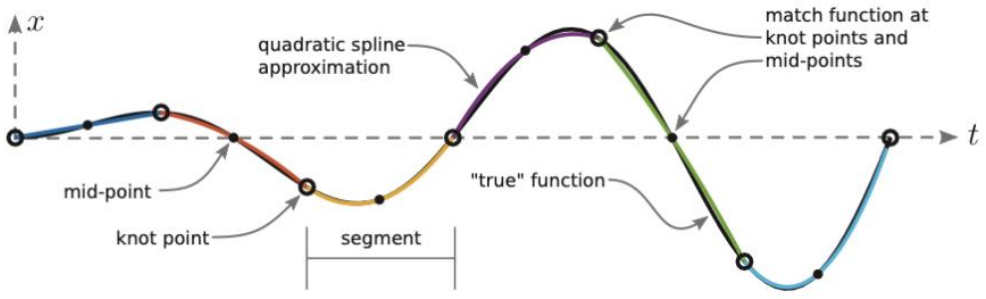


Figure 3.4 Function Approximation using a Quadratic Spline [26] (Notice that this approximation is far more accurate than the linear spline in Figure 3.2, for the same number of segments)

3.1.6 Formulation of Trajectory Optimization

States and input variables of the optimal control problem to be solved here are given below.

$$x^T = [x_m, y_m, z_m, V_m, \gamma_m, \eta_m] \tag{3.14}$$

$$u^T = [a_\gamma, a_\eta] \tag{3.15}$$

Table 3.1 Upper and Lower Bounds for the States of the Missile

Parameter	**Lower Bound**	**Upper Bound**	**Unit**
x_m	-10^6	10^6	m
y_m	-10^6	10^6	m
z_m	0	30000	m
V_m	200	2000	m/s
γ_m	-2π	2π	rad
η_m	-2π	2π	rad

The majority of states possess high levels of freedom. That is why some of the entries have exaggerated values in Table 3.1. The most significant constraints are the limitations on z_m and V_m. The vertical coordinate z_m should be positioned at an elevation above sea-level, thereby representing the minimum value. However, the upper limit is established to prevent entering stratosphere layer. The higher bound for V_m is irrelevant as the missile is incapable of attaining such a speed, however the lower bound is significant. Its purpose is to guarantee a minimum velocity during the flight. If this minimum velocity is not maintained in a realistic situation, the likelihood of successfully intercepting the target would be greatly reduced due to either no closing velocity or a negative closing velocity [8].

The path (nonlinear state inequality) constraints are as written below.

$$-35g \leq \sqrt{a_\gamma^2 + a_\eta^2} \leq 35g \tag{3.16}$$

$$-15° \leq \alpha \leq 15° \tag{3.17}$$

$$-30° \leq \delta_1, \delta_2, \delta_3, \delta_4 \leq 30° \tag{3.18}$$

The boundary (terminal inequality) constraint is

$$\sqrt{(x_t - x_m)^2 + (y_t - y_m)^2 + (z_t - z_m)^2} \leq 10\ km \tag{3.19}$$

The objective function is defined as

$$J = \min_{x(t),u(t)} \{t_f + \mu_\lambda |\lambda_z| + \mu_\lambda |\lambda_y|\} \tag{3.20}$$

Recall that λ_z and λ_y are the line-of-sight angles in the pitch and yaw planes that occur as the missile enters the spherical manifold of the terminal guidance phase, i.e., as the PNG phase starts. As for μ_λ, it is the weighting coefficient. In the proposed hybrid guidance method, μ_λ is taken as unity. Depending upon the proposed method's desired objective and scenario of use, various μ_λ values can be employed to either restrict sudden changes in acceleration commands more strictly or to enable more freedom.

The built-in "fmincon" function of MATLAB in the optimization toolbox is an effective method for minimizing a performance index, subject to both linear and nonlinear equality and inequality constraints [29]. The options used in the study are selected as given below.

Table 3.2 “fmincon” Options Used in Simulations

Algorithm	**‘TolFun’**	**‘MaxIter’**	**‘MaxFunEvals’**	**Grid Number**
Interior-point	1e-6	5e4	5e4 * (Number of state grids + Number of control grids)	30

The meanings of the terms in Table 3.2 are explained below.

TolFun: Termination tolerance for the function value (a positive scalar).

MaxIter: Maximum number of iterations allowed, a positive integer.

MaxFunEvals: Maximum number of function evaluations allowed, a positive integer.

It is important to find proper grid number to converge optimal results. Multiple simulations have demonstrated that using 30 grids happens to be enough to practically attain the optimal outcome.

- **Notes about Optimization with Updates of Target’s Data**

The optimization tool is provided with starting estimates for the state and control inputs of the optimal control problem, as well as the flight time estimation, based on the known locations and speeds of the missile and target at time t_0. In this initial estimation, the total flight time is divided by the number of grids and allocated evenly to each grid. Next, an evaluation is conducted to see if the outcomes achieved using these divided time intervals agree to the constraints and boundaries. The solution method is iterated until an improved estimate of the flight time and values that meet both the shortest flight time and the given constraints are achieved. As the missile and target continue their trajectory, as new information received from the ground

station, the shortest flight time found in the last step is taken as the first flight time estimate of the new solution, and the shortest flight time that meets the constraints and limits for the new positions and speeds is found as in the previous step.

3.2 Standart Proportional Navigation Guidance – Terminal Phase

Proportional navigation guidance (PNG) is the most widely used law in practice. The basic philosophy behind PNG is that missile acceleration should nullify the rate of the line-of-sight (LOS) angle between the target and interceptor [30]. In PNG, it is necessary for the rate of the line-of-sight (LOS) angle to be precisely zero. Actually, this rate is not zero. Therefore, the guiding acceleration commands, which are proportional to the rate of change of the line of sight (LOS) angle, will reduce the absolute value of this rate and make it approach zero. The PNG law states that the constant of proportionality can be expressed as the product of the effective navigation ratio N and the relative velocity of the missile and the target as they approach each other. See Equation (3.21) for the expression of this proportionality. A typical engagement scenario is illustrated in Figure 3.5, where the target is a rectilinearly flying aircraft.

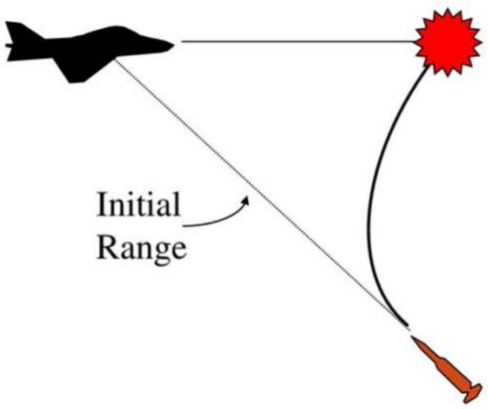


Figure 3.5 Sketch of a Simple Engagement with PNG [32]

The terminal phase starts when the range between the missile and target becomes less than $10\ km$. In the terminal phase, the sensors of the target such as radars can detect the approaching missile. Then, the target may start to perform last ditch maneuvers (to be defined in Chapter 4). From the missile's point of view, to focus on minimizing the miss distance and increasing the hit probability, the proportional navigation guidance is preferred, which is formulated as

$$a_c = NV_c\dot{\lambda} \tag{3.21}$$

Actually, the PNG problem should be formulated as a three-dimensional control problem. By assuming that the lateral and longitudinal maneuver planes are decoupled through a proper roll control, it becomes feasible to simplify the three-dimensional guidance problem into almost identical two-dimensional planar problems [30].

In all PNG calculations in the present work, $N = 5$ is taken as the cruise/navigation coefficient. The distances between the missile and the target in the lateral and longitudinal planes are calculated as

$$R_y = \sqrt{(x_t - x_m)^2 + (y_t - y_m)^2} \tag{3.22}$$

$$R_z = \sqrt{(z_m - z_t)^2 + (R_y)^2} \tag{3.23}$$

The line-of-sight angles in the lateral and longitudinal planes are found as

$$\lambda_y = atan2((y_t - y_m), (x_t - x_m)) \tag{3.24}$$

$$\lambda_z = -atan((z_m + z_t)/R_y) \tag{3.25}$$

The closing velocities in the lateral and longitudinal planes happen to be

$$V_{c,y} = \left(V_{m,x} - V_{t,x}\right) cos\left(\lambda_y\right) + \left(V_{m,y} - V_{t,y}\right) sin\left(\lambda_y\right) \tag{3.26}$$

$$V_{c,z} = V_{c,y}\, cos(\lambda_z) - \left(V_{m,z} - V_{t,z}\right) sin(\lambda_z) \tag{3.27}$$

Hence, the rates of the line-of-sight angles in the lateral and longitudinal planes are obtained as

$$\dot{\lambda}_y = \frac{\left(V_{m_x} - V_{t_x}\right) sin\left(\lambda_y\right) - \left(V_{m_y} - V_{t_y}\right) cos\left(\lambda_y\right)}{R_y} \tag{3.28}$$

$$\dot{\lambda}_z = \frac{V_{c_y}\, sin(\lambda_z) + \left(V_{m_z} - V_{t_z}\right) cos(\lambda_z)}{R_z} \tag{3.29}$$

Finally, the acceleration commands in the lateral and longitudinal planes are generated as

$$a_\eta = N V_{c_y} \dot{\lambda}_y \tag{3.30}$$

$$a_\gamma = NV_{c_z}\dot{\lambda}_z - gcos(\gamma_m) \quad (3.31)$$

3.3 Reference Guidance Law – PN Guidance with Lofting

To compare performance of proposed guidance law, the PN guidance law is considered as baseline since most of the missiles use different forms of PN guidance due to its computational simplicity.

Here, it is to be pointed out that the conventional PN guidance law could not be sufficient to form a proper trajectory shaping for the missile because it aims to minimize the final distance to the target by considering solely the rate of the line-of-sight angle without paying attention to the termination speed. For instance, to achieve missions with longer ranges in shorter amounts of time, a proper trajectory shaping mechanism must make the missile climb to higher altitudes by taking into account that the atmosphere becomes less dense at higher altitudes resulting in reduced drag [8].

To elevate the missile, either an initial elevation angle is provided, or a g-bias is introduced to the acceleration command obtained by the plain PN guidance law [14]. In the literature of guidance and control area, there is no established method for designing an ideal g-bias schedule. Therefore, the only option is to use a trial-and-error approach in order to minimize both the flight time and the miss distance. To find the amount of the g-bias, it is aimed that the maximum altitude attained by the proposed hybrid guidance method is also attained closely by the PN guidance with lofting.

Mathematically, the PN guidance with lofting law is presented as below.

No bias is introduced to the lateral acceleration command; however, a bias term adequate to elevate the missile to the same altitude using the proposed hybrid guidance method is applied to the longitudinal acceleration over a period of time sufficient to achieve this elevation.

$$a_\gamma = NV_{c_z}\dot{\lambda}_z - gcos(\gamma_m) + bias\ term \tag{3.32}$$

CHAPTER 4

SIMULATION WORK

The simulation work chapter demonstrates the performance of the proposed hybrid guidance methods, which includes optimal midcourse and terminal with PN guidance phases. To conduct a performance comparison, the biased version of PNG as explained in Chapter 3 is employed since PN guidance is widely recognized, utilized, and approved in the guidance and control area. The level of bias is established based on the lofting height criterion to ensure a fair comparison.

The simulation model is constructed by utilizing the MATLAB software, employing the modeling works and guidance methods described in the preceding chapters.

During the simulation studies, the criterion for success is defined as the missile's ability to stay within a circular area with a radius of $10\ m$ around the target until the ending of the simulation. In other words, acceptable miss distances are less than $10\ m$.

In the doctrine of air-to-air combat, there are mainly three types of engagement scenarios for a beyond-visual-range air-to-air missile and target:

Head-On Engagements: In the head-on scenarios, as obvious from the name, the pursuer (missile) and the evader (target) move towards each other until the moment of collision. Different closing velocities, target acceleration, range, and altitude difference can be used to diversify the scenarios for simulation studies.

Tail-Chase Engagements: In this type of scenarios, the target runs away from the missile with almost 0° azimuth angle difference, i.e., $\Delta\eta = \eta_t - \eta_m \cong 0$. Again, the number of scenarios can be increased by changing aforementioned parameters.

Turn-and-Run Maneuvers: Turn-and-Run is an evasive maneuver done by target when it detects the approaching missile. When the distance between the pursuer and evader is below a pre-defined radar range, the evader maneuvers with a lateral acceleration which is perpendicular to its velocity vector.

Aside from the ones described above, there are also last-ditch maneuvers, which are aggressive maneuvers used to avoid a BVRAAM getting closer to the target for impact. These maneuvers are typically used when other defensive tactics, such as electronic countermeasures, chaff, flares, or earlier evasive actions, have been found to be unsuccessful or insufficient. When the distance between the pursuer and evader becomes significantly close, the evader makes sudden changes in direction or speed. As a measure of evasive maneuvers' limit, modern fighter jets are often engineered to endure g-forces of up to 9 g [33].

The precise g-limit for executing a "Last Ditch" maneuver would be contingent upon the unique characteristics of the aircraft's design and its range of permissible flight conditions. As an example, an F-16 Fighting Falcon or an F/A-18 Hornet can normally withstand accelerations of up to 9 g. An F-22 Raptor or an F-35 Lightning II may exhibit equivalent or slightly higher capabilities in terms of g-limits and sustained high-g maneuvers.

In the Case 1 of simulation studies, it is aimed to demonstrate that the proposed guidance method effectively prevents sudden changes in acceleration commands. The proposed hybrid guidance method, which includes an optimal entry point with an optimal line-of-sight (LOS) angle to the terminal phase, is compared to the same method without optimal entrance.

In the Cases 2,3 and 4, performance comparison between the proposed guidance method and PN guidance with lofting is done in terms of flight time and impact speed by usign the engagement scenarios explained above.

4.1 Case 1 – Nonmoving Target Engagement

Table 4.1 Initial Conditions of Case 1 – Nonmoving Target Engagement

Initial Conditions (t_0)	**Missile**	**Target**
$x\ (km)$	-100	0
$y\ (km)$	0	0
$h\ (km)$	6	6
$Velocity\ (m/s)$	300	0
$Heading\ (Azimuth)\ (°)$	0	0
$Elevation\ (°)$	0	0
$Last\ Ditch\ Maneuver$	–	

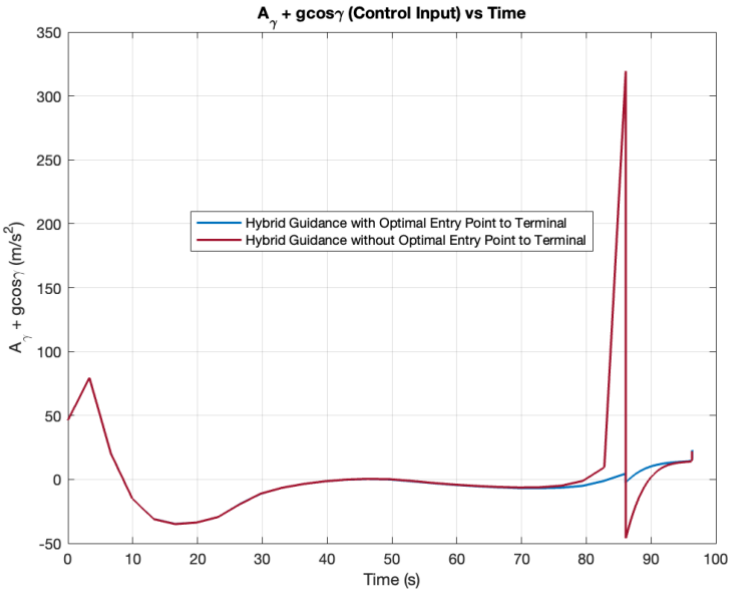


Figure 4.1 Elevational Acceleration of the Missile vs Time – Nonmoving Target Engagement

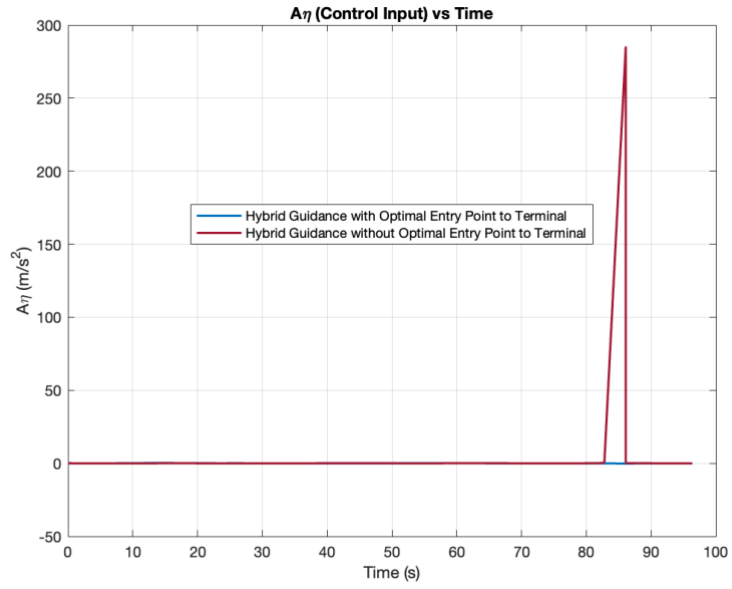


Figure 4.2 Lateral Acceleration of the Missile vs Time – Nonmoving Target Engagement

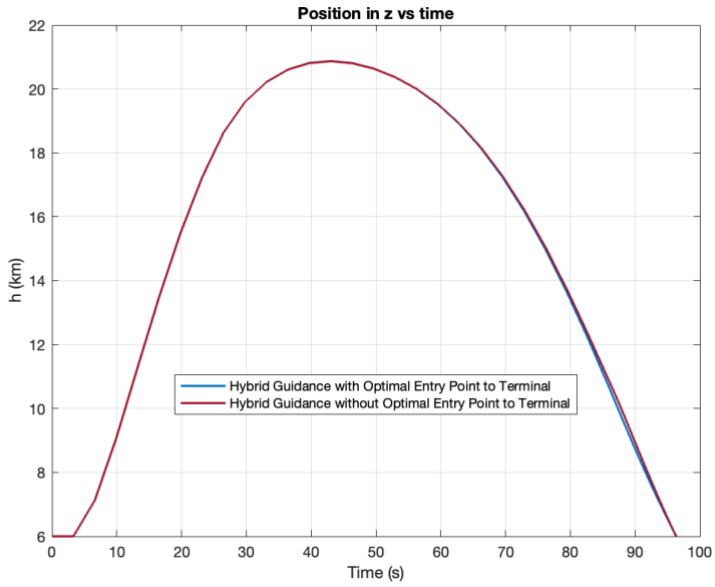


Figure 4.3 Altitude of the Missile vs Time – Nonmoving Target Engagement

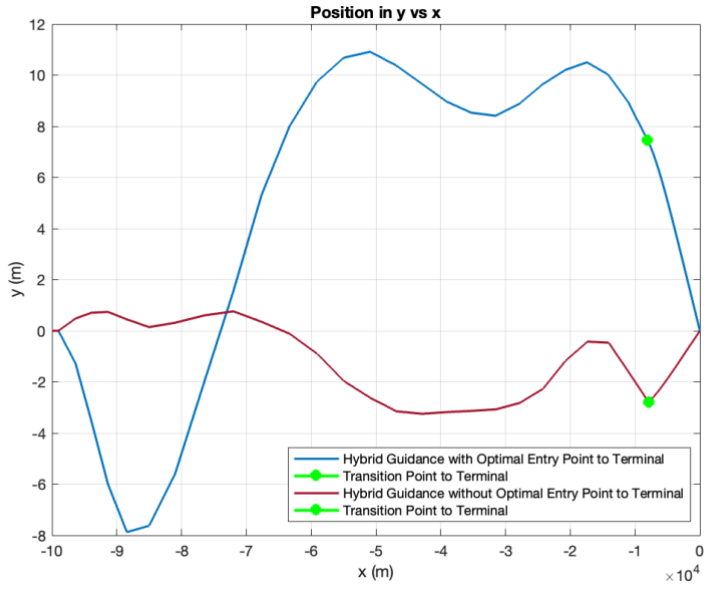


Figure 4.4 y Position vs x Position of the Missile – Nonmoving Target Engagement

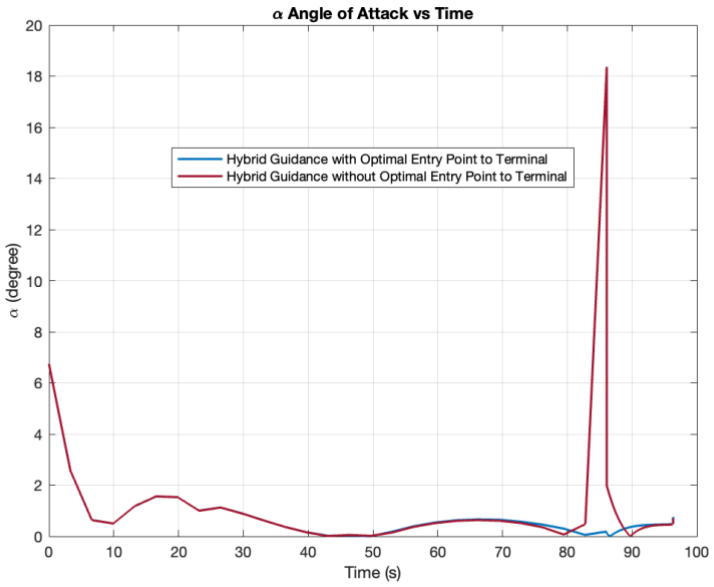


Figure 4.5 Angle of Attack vs Time – Nonmoving Target Engagement

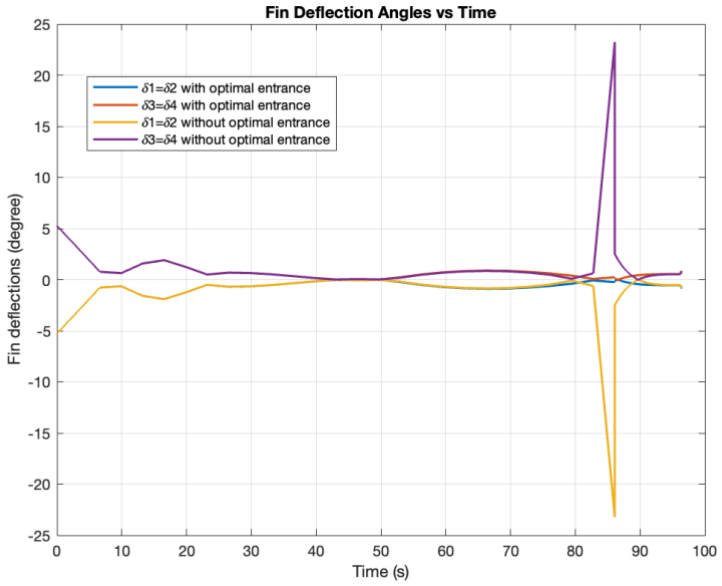


Figure 4.6 Fin Deflection Angles vs Time – Nonmoving Target Engagement

The advantages of achieving the optimal line-of-sight angle at the entry of the terminal phase are evident, as they significantly simplify the duties of the autopilots and the control actuation systems. On the other hand, as an expected result, decreasing the acceleration required during the transition lowers the speed at which impact occurs. Decreased accelerations can prevent the pursuit of higher speeds or retaining current speed.

Table 4.2 Results of Nonmoving Target Engagement Simulation

Guidance Law	**Entry Time to Terminal**	**Entry Speed to Terminal**	**Time of Flight**	**Impact Speed**	**Miss Distance**
Hybrid Guidance Law with Optimal Terminal Entry	86.05 s	3.31 $Mach$	96.36 s	2.15 $Mach$	1.16 m
Hybrid Guidance Law without Optimal Terminal Entry	86.09 s	3.32 $Mach$	96.32 s	2.60 $Mach$	1.41 m

4.2 Case 2 – Turn and Run Engagement

Table 4.3 Initial Conditions of Case 2 – Turn and Run Engagement

Initial Conditions (t_0)	**Missile**	**Target**
$x\ (km)$	-100	0
$y\ (km)$	0	0
$h\ (km)$	6	6
$Velocity\ (m/s)$	300	250
$Heading\ (Azimuth)\ (°)$	0	180
$Elevation\ (°)$	0	0
$Last\ Ditch\ Maneuver$	Turn-and-Run Maneuver with lateral 7 g when the range is less than 10 km	

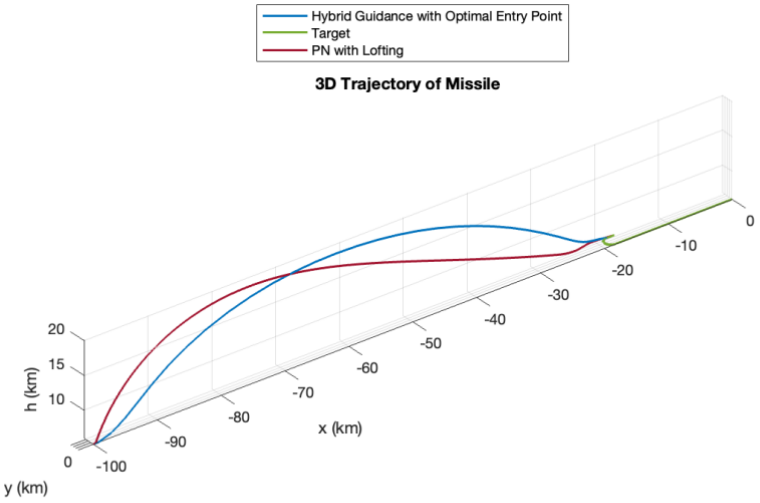


Figure 4.7 3D Trajectory of the Missile – Turn and Run Engagement

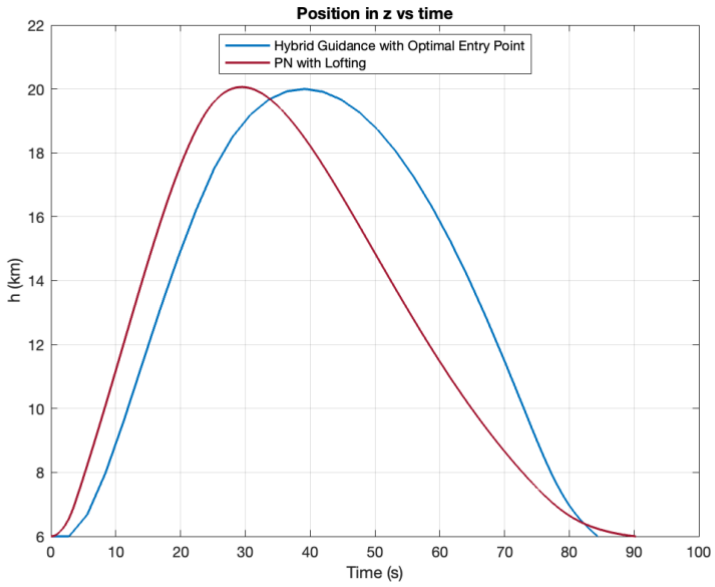


Figure 4.8 Altitude of the Missile vs Time – Turn and Run Engagement

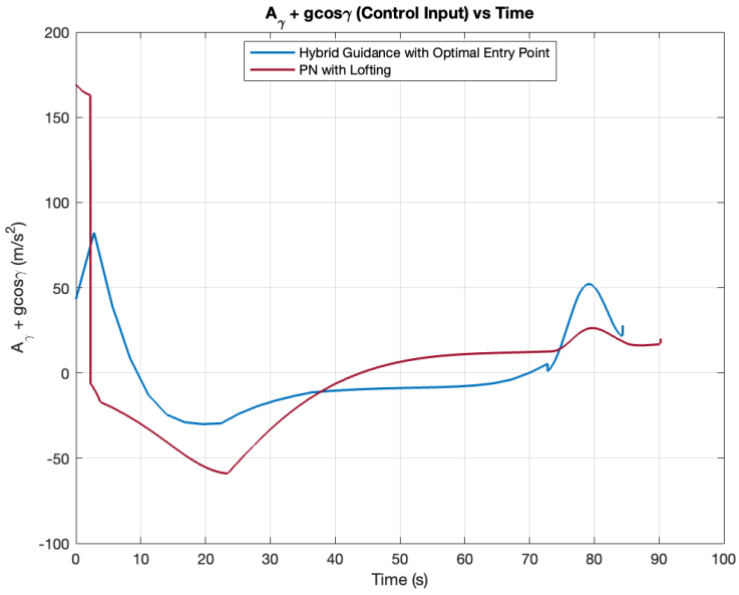


Figure 4.9 Elevational Acceleration of the Missile vs Time – Turn and Run Engagement

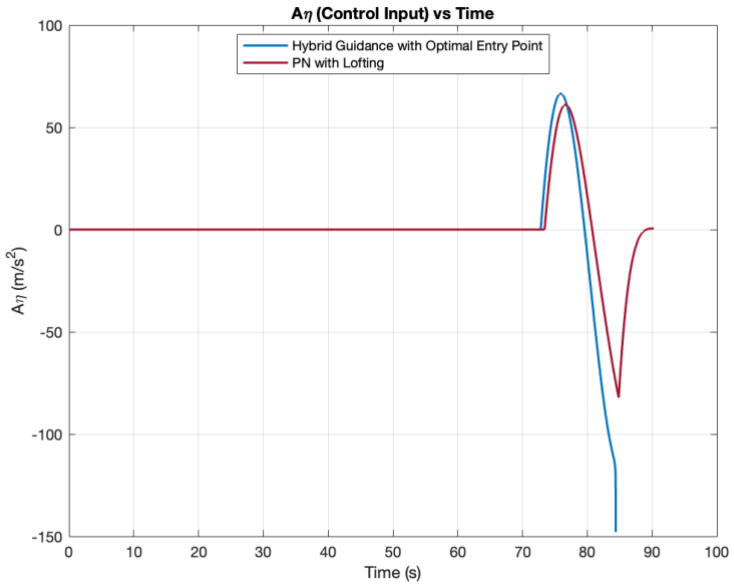


Figure 4.10 Lateral Acceleration of the Missile vs Time – Turn and Run Engagement

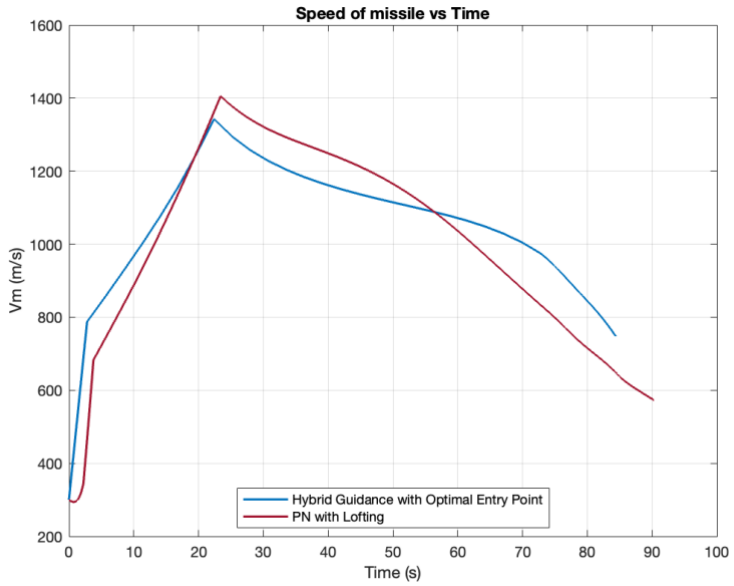


Figure 4.11 Speed of the Missile vs Time – Turn and Run Engagement

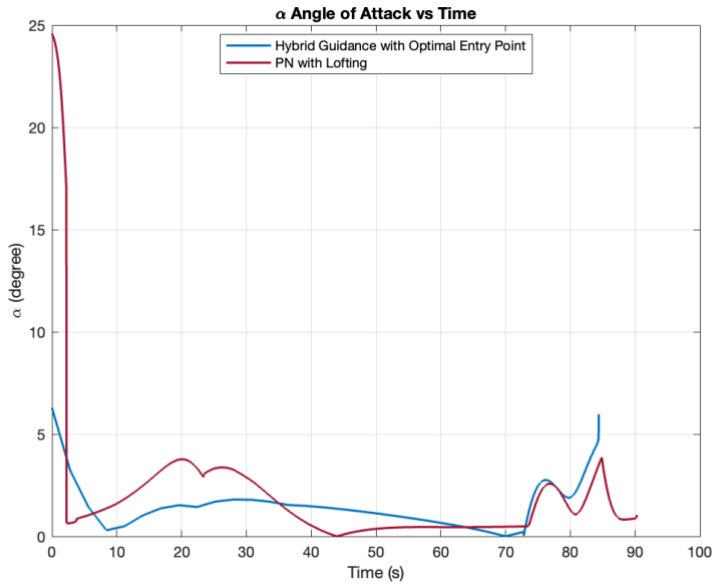


Figure 4.12 Angle of Attack vs Time – Turn and Run Engagement

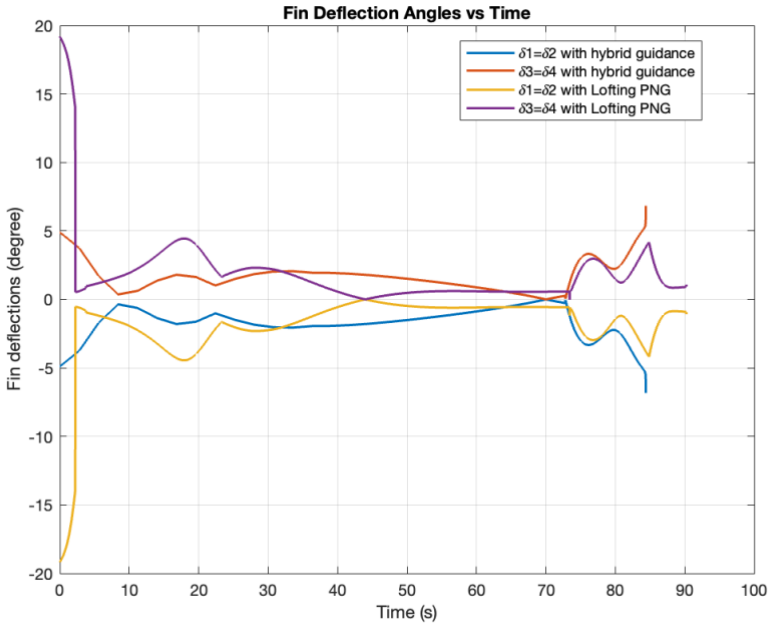


Figure 4.13 Fin Deflection Angles vs Time – Turn and Run Engagement

Table 4.4 Results of Turn and Run Engagement Simulation

Guidance Law	**Entry Time to Terminal**	**Entry Speed to Terminal**	**Time of Flight**	**Impact Speed**	**Miss Distance**
Hybrid Guidance Law with Optimal Terminal Entrance	72.80 s	3.26 $Mach$	84.39 s	2.36 $Mach$	3.40 m
PN Guidance Law with Lofting	73.41 s	2.67 $Mach$	90.26 s	1.81 $Mach$	6.94 m

Figure 4.9 illustrates the amount of g-bias added to the longitudinal acceleration command of PN guidance with lofting, as well as its duration. In the turn and run scenario, $17.25g$ is added to the command during the first $2.25\ seconds$ of the flight. Then, the maximum altitude reached by the proposed method is also achieved by the PN guidance with lofting.

The results of turn and run engagement simulation demonstrate the superiority of hybrid guidance with optimal terminal entrance in terms of the flight time and impact speed. Actually, the superiority is attained by acquiring the speed profile illustrated in Figure 4.11. This hybrid method enables the missile to utilize its speed more effectively. Moreover, the proposed method enables the missile to hit the target from a smaller distance compared to PN guidance with lofting. While adhering to the constraints of angle of attack and fin deflections, the proposed method achieves these improvements in performance.

4.3 Case 3 – Head-On Engagement

Table 4.5 Initial Conditions of Case 3 – Head-On Engagement

Initial Conditions (t_0)	**Missile**	**Target**
$x\ (km)$	-100	0
$y\ (km)$	0	0
$h\ (km)$	6	6
$Velocity\ (m/s)$	300	250
$Heading\ (Azimuth)\ (°)$	0	180
$Elevation\ (°)$	0	0
$Last\ Ditch\ Maneuver$	Last Ditch Maneuver with lateral 8 g and longitudinal 3 g when the range is less than 10 km	

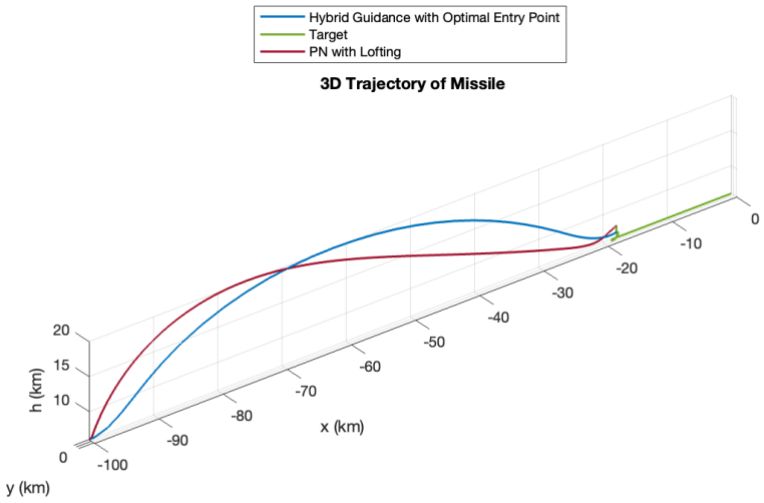


Figure 4.14 3D Trajectory of the Missile – Head-On Engagement

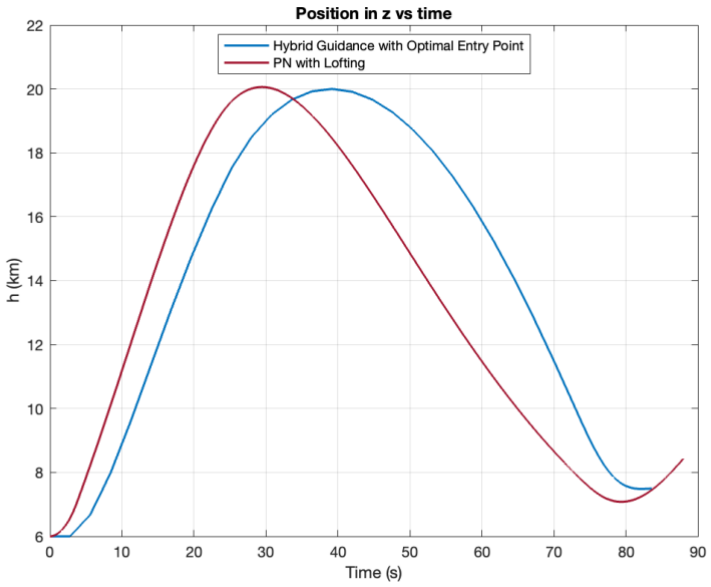


Figure 4.15 Altitude of the Missile vs Time – Head-On Engagement

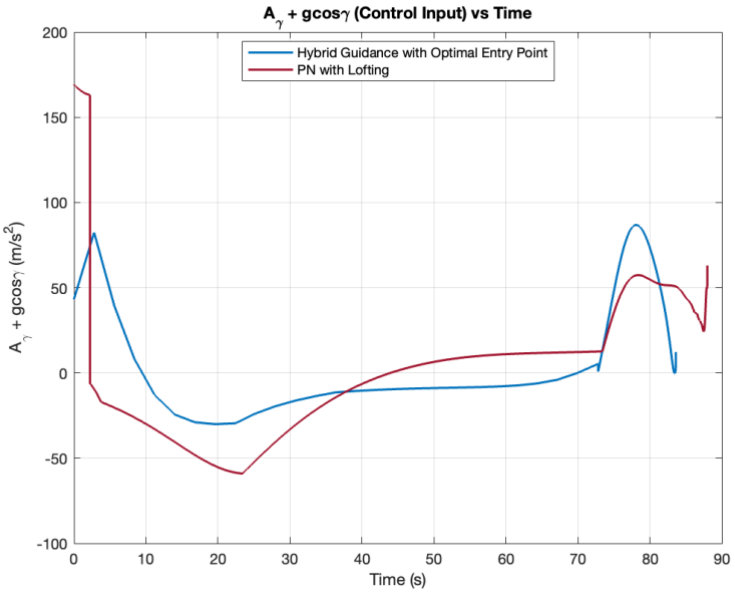


Figure 4.16 Elevational Acceleration of the Missile vs Time – Head-On Engagement

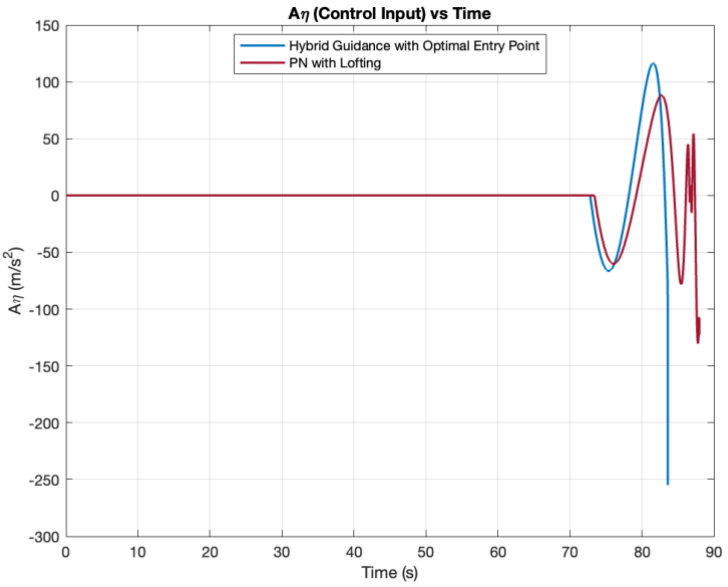


Figure 4.17 Lateral Acceleration of the Missile vs Time – Head-On Engagement

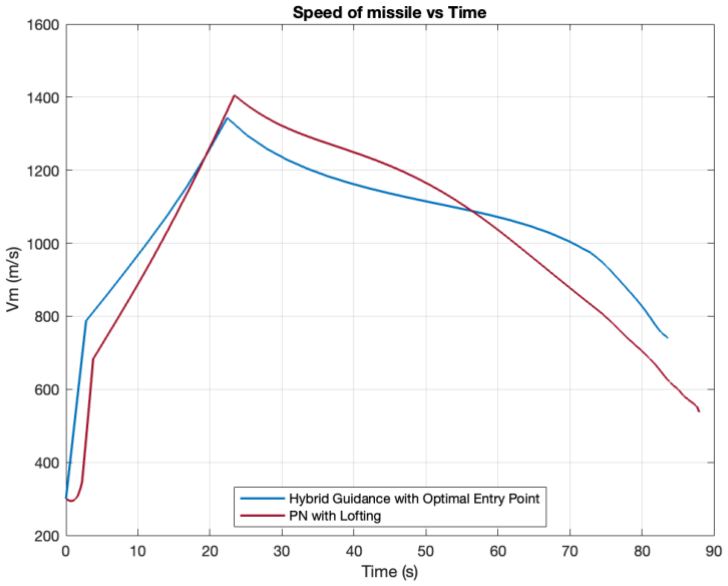


Figure 4.18 Speed of the Missile vs Time – Head-On Engagement

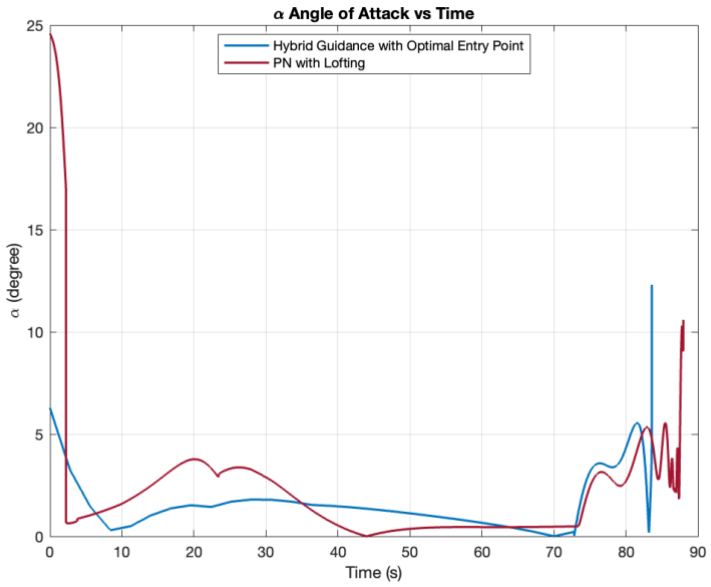


Figure 4.19 Angle of Attack vs Time – Head-On Engagement

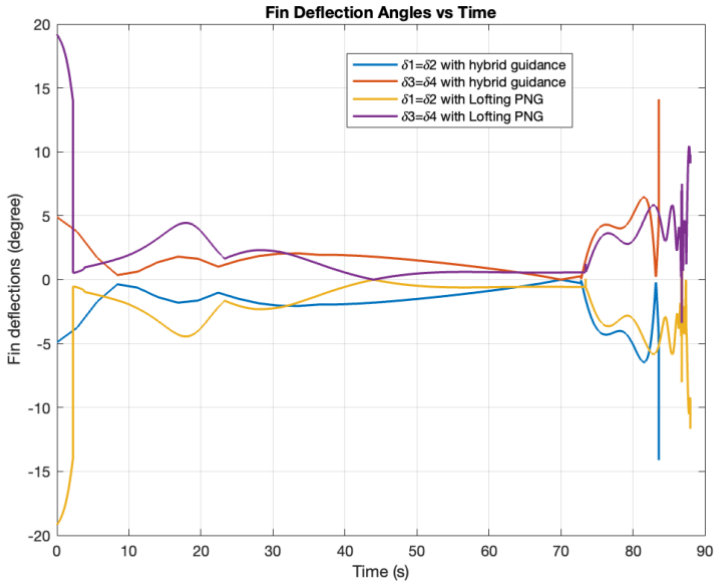


Figure 4.20 Fin Deflection Angles vs Time – Head-On Engagement

Table 4.6 Results of Head-On Engagement Simulation

Guidance Law	Entry Time to Terminal	Entry Speed to Terminal	Time of Flight	Impact Speed	Miss Distance
Hybrid Guidance Law with Optimal Terminal Entrance	72.80 s	3.26 $Mach$	83.60 s	2.38 $Mach$	3.14 m
PN Guidance Law with Lofting	73.41 s	2.67 $Mach$	87.99 s	1.76 $Mach$	7.13 m

According to Figure 4.16, a bias $17.25g$ is added to the longitudinal command during the starting 2.25 $seconds$ of the flight.

The head-on engagement scenario with last-ditch maneuvers continues to illustrate the advantages of the hybrid guidance approach.

4.4 Case 4 – Tail-Chase Engagement

Table 4.7 Initial Conditions of Case 4 – Tail-Chase Engagement

Initial Conditions (t_0)	Missile	Target
$x\ (km)$	-100	0
$y\ (km)$	0	0
$h\ (km)$	6	6
$Velocity\ (m/s)$	300	250
$Heading\ (Azimuth)\ (°)$	0	0
$Elevation\ (°)$	0	0
$Last\ Ditch\ Maneuver$	–	

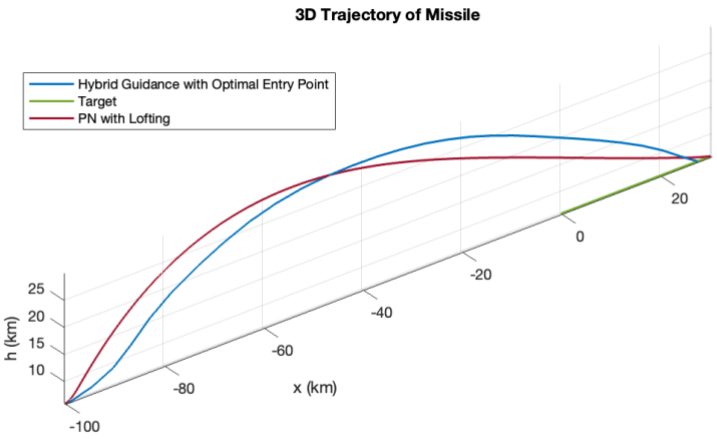


Figure 4.21 3D Trajectory of the Missile and the Target – Tail-Chase Engagement

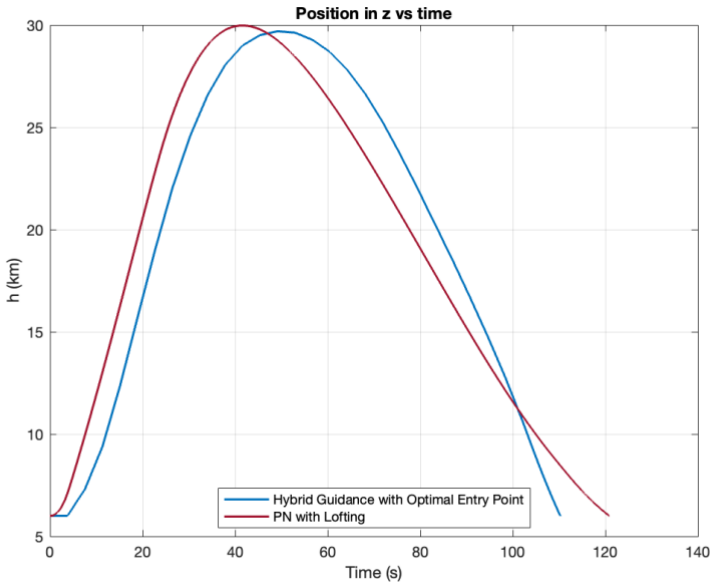


Figure 4.22 Altitude of the Missile vs Time – Tail-Chase Engagement

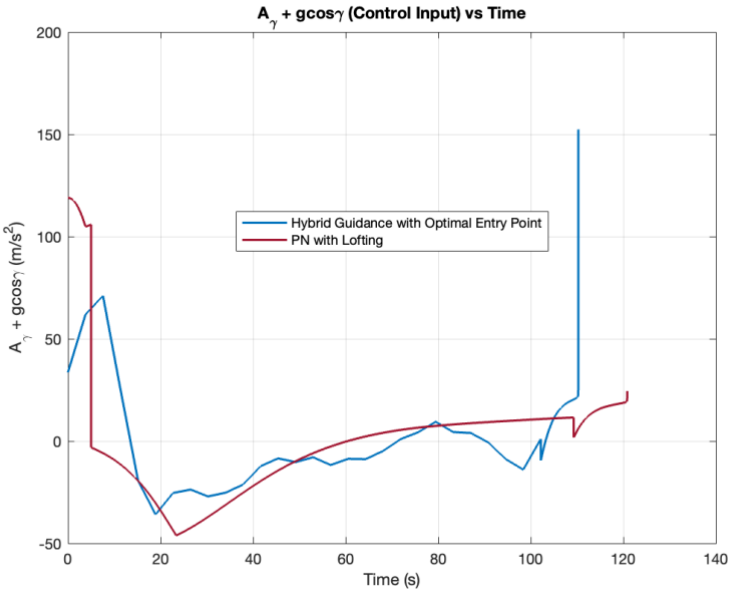


Figure 4.23 Elevational Acceleration of the Missile vs Time – Tail-Chase Engagement

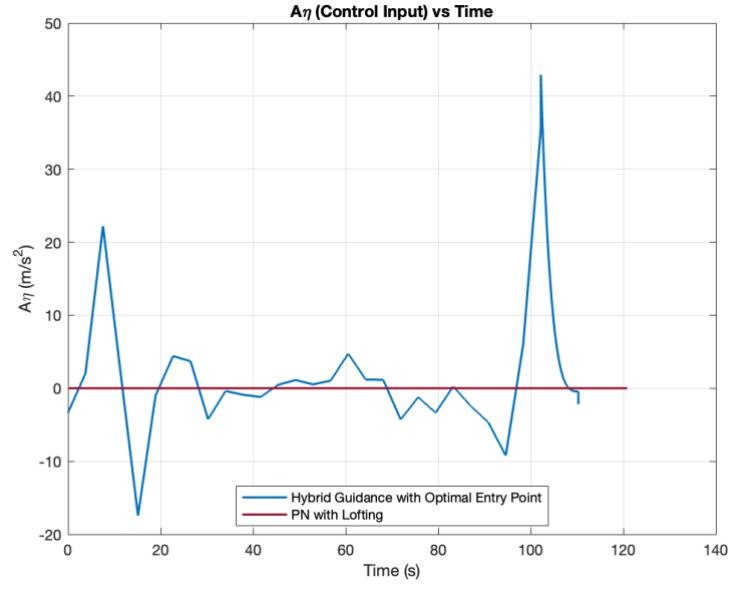


Figure 4.24 Lateral Acceleration of the Missile vs Time – Tail-Chase Engagement

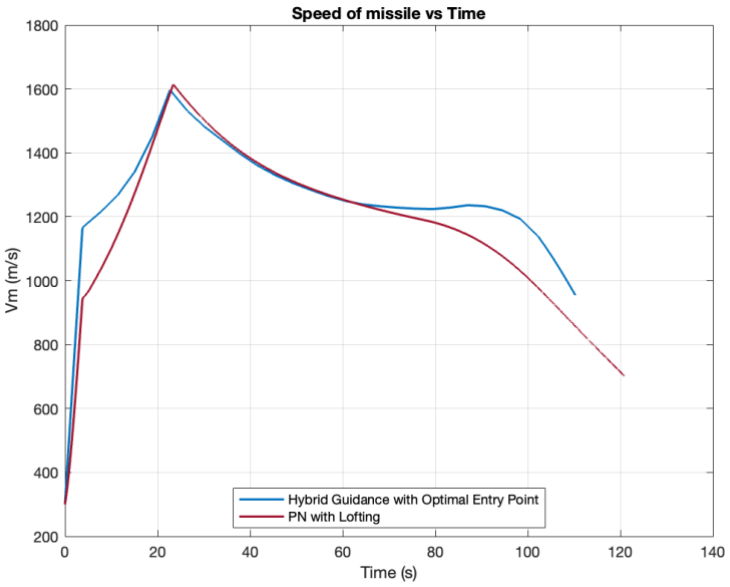


Figure 4.25 Speed of the Missile vs Time – Tail-Chase Engagement

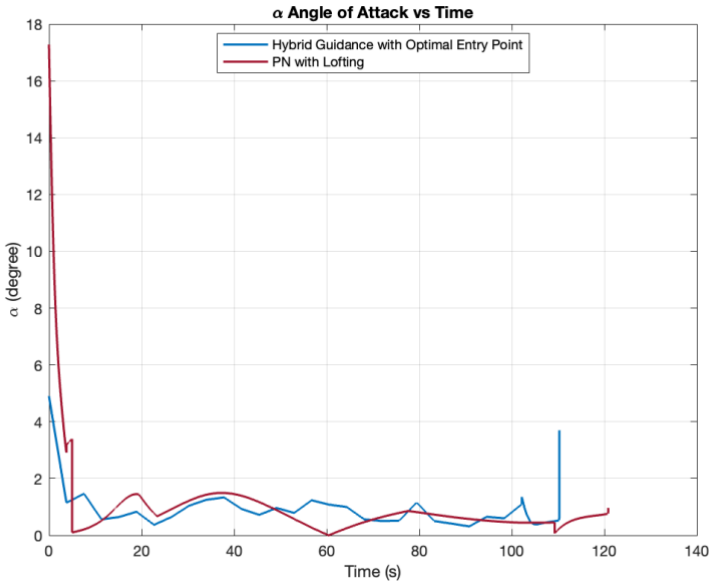


Figure 4.26 Angle of Attack vs Time – Tail-Chase Engagement

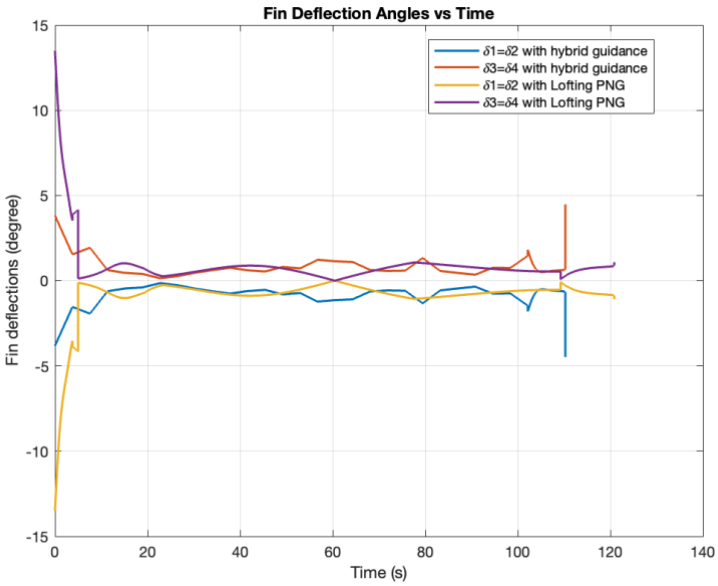


Figure 4.27 Fin Deflection Angles vs Time – Tail-Chase Engagement

Table 4.8 Results of Tail-Chase Engagement Simulation

Guidance Law	**Entry Time to Terminal**	**Entry Speed to Terminal**	**Time of Flight**	**Impact Speed**	**Miss Distance**
Hybrid Guidance Law with Optimal Terminal Entrance	102.16 s	3.84 $Mach$	110.28 s	3.02 $Mach$	4.48 m
PN Guidance Law with Lofting	104.00 s	3.19 $Mach$	120.86 s	2.22 $Mach$	8.05 m

Figure 4.24 illustrates that the lateral accelerations of the proposed method variate while the other one's remain zero. The purpose of this dynamic trend is to produce

the speed profile depicted in Figure 4.25, which is facilitating the achievement of the shortest possible flying time and the highest achievable terminal kinetic energy.

As seen in Figure 4.23, $12.125g$ is added to the longitudinal command during the initial 5 seconds. Then, a $1g$ bias term is employed until the last $10\ seconds$ of the flight.

Again, this simulation scenario demonstrates that the proposed method is advantageous regarding the aforementioned performance characteristics while complying with the specified constraints.

CHAPTER 5

CONCLUSION AND FUTURE WORKS

The primary objective of this study is to create and refine guidance algorithms specifically designed for beyond-visual-range air-to-air missiles (BVRAAM). Its objective is to enhance the missile guidance system for use in modern air-to-air combat. This study has enhanced the optimization of BVRAAM guidance by leveraging the benefits of earlier research in the literature. In addition to that, the hardware constraints related to the control actuation system and the ramjet engine are considered by guidance algorithm in a more extensive manner compared to earlier studies.

5.1 Conclusion

The first part of this thesis primarily focuses on modeling work. The missile is represented as a particle. The modeling process involves a systematic step-by-step approach, where the necessary transformations are performed between the reference coordinate frames using the related angles. Ultimately, the kinematic and dynamic equations that describe the motion of the missile are derived.

Next, the concept of bank-to-turn (BTT) flight is discussed, along with the method of controlling a missile using this principle. This involves providing two acceleration commands as inputs to the related equations of motion. It is underlined that in missiles that fly using the principle of bank-to-turn, the side slip angle, side force, and rudder deflection are around zero. This part also demonstrates the methodology for determining the angle of attack and elevator deflection, which are crucial parameters for a BVRAAM's constraints.

The next subheading briefly mentions the explanation of thrust force, as well as a summary of how ramjet engines work and their operational envelope. The ramjet engine requires the ignition of a rocket engine to achieve its working speed. Simplified formula and pertinent parameters for calculating the thrust force are given. The significance of ramjet technology in the context of a long-range air-to-air missile is also emphasized.

The subsequent section provides the geometric characteristics of the missile as input, resulting in the acquisition of an aerodynamic database for a high-performance missile using the Missile DATCOM tool. The database stores aerodynamic force and moment coefficients as functions that are dependent on characteristics such as angle of attack, sideslip angle, and Mach number. The procedure for determining the air density and pressure required for computing the aerodynamic force is also demonstrated. The drag force is obtained by using the lift force based on the control accelerations of the missile.

The final subheadings of the modeling section include the roll autopilot which is employed to obtain aileron deflections with the second-order basic control actuation system model. Also, the kinematic model of the target used in simulation studies is presented.

The second primary heading of the thesis encompasses the methodologies employed for guidance in this study. An explanation of the distinction between midcourse and terminal guidance phases is provided. The modeling of midcourse guidance involves formulating it as an optimal control problem and solving it using nonlinear programming via direct collocation methods. The theory behind these techniques and approaches is elucidated, and the state and input variables of the optimal control problem are precisely described. Constraints and boundaries pertaining to the state and control variables and hardware, such as ramjet and fins, are given. Additionally, the options of MATLAB's "fmincon" function, employed as a solution tool, are provided.

In the second section of this thesis, the principles and development of the typical Proportional Navigation Guidance (PNG) employed throughout the terminal phase of guidance are presented. Next, the use of the biased PN guidance – PN guidance with lofting law is described, which serves as a reference method in simulation studies. The reason is that the standard PN guidance explained in Chapter 3.2 is the most prevalent and extensively utilized guidance law. Consequently, it is considered suitable for a rule deriving from PNG to serve as the reference method for comparison. Specifically, the rule pertaining to the amount of bias is discussed for the sake of a reasonable comparison.

The following section elucidates the engagement types utilized in simulation studies and frequently encountered in modern air-to-air combats. The first simulation utilizes a nonmoving target model to elucidate methods for minimizing the sudden increase in acceleration and other related flight parameters that occur during the transition from the midcourse to the terminal guidance phase. The remaining simulations confirm the superiority of the suggested hybrid guidance method in terms of flight time, impact speed and miss distance compared to the PN guidance with lofting. MATLAB software is employed to carry out all simulation studies.

At the beginning of this work, the expectations are obtaining improvements in the performance of a BVRAAM's guidance in terms of flight time and impact speed compared to the reference method mentioned in Chapter 3.3. Moreover, the optimal midcourse guidance is expected to consider the transition between the midcourse and terminal phases in case of sudden changes in the acceleration commands. The results of simulation work show that the expectations are met. For all simulation cases, substantial amount of kinetic energy is retained in the terminal phase, enhancing the efficiency of PN guiding against the target's evasive maneuvers, owing to the optimal midcourse phase. As mentioned previously, beside the enhancement of performance metrics regarding flight time, impact speed, and maneuverability, the hardware limitations of the ramjet engine and control actuation systems are incorporated into the proposed guidance method as constraints of the optimal midcourse problem. In all the simulation cases, the constraints are adhered.

The proposed method is feasible to implement readily if the processors have adequate computational performance since the guidance algorithms are embedded in the processors. Therefore, the proposed method might not be used in an online manner during the flights due to computational burden. To reduce the computational burden and increase feasibility of proposed method, the midcourse phase can be posed and solved in a suboptimal manner. Results of suboptimal methods, which rely on certain assumptions and neglect various factors, deviate slightly from optimal results; nonetheless, they may be favored due to their accelerated and simplified solutions. Also, online computations can be reduced by means of some kind of simple online interpolation methods based on a set of offline precomputations. Instead of optimizing online during the flight, interpolating between the scheduled versions of the results derived from offline precomputations would be simpler for the processor.

The optimization tool which is the “fmincon” built-in function of the MATLAB provides a local minimum. The global minimum is the minimum value attained in all locations where an objective function is defined. In other words, it is the minimum value of the objective function. A local minimum is the lowest value attained by an objective function within a certain region. Although there may be lower values in other parts of the function, this minimum represents the lowest value within that specific region. Identifying a global minimum usually results in better results as it implies obtaining the objective function's lowest value. Identifying a considerably lower global minimum may yield a performance improvement. Still, if the local minimum and global minimum values are in proximity to each other, the performance improvement may be very limited. Also, local minimums are typically easier and faster to find. Increased computational power and time may be necessary when pursuing a global minimum. To reach the global minimum, alternative tools may be explored such as “GlobalSearch” built-in function of the MATLAB software.

5.2 Future Works

In future works,

- The outcomes of simulation experiments undertaken with a significantly broader set of cases can be consolidated. One can analyze BVRAAM guidance using "neural network" techniques to determine the most effective flight paths in an online manner. These studies involve combining several factors such as the target's location, velocity, and path, which can serve as inputs to make decisions while in the air. The outcomes may consist of the acceleration commands required to be used by the missile's autopilots.

- More subsystems and sensors can be included in the optimal control problem as constraints throughout the optimization process. For example, an additional constraint can be posed on the angle between the transmitter and the missile so that it is maintained within a certain range to ensure uninterrupted datalink information flow and keeping the line-of-sight angle within a specific range to optimize the efficiency of the missile seeker. As another example, data link model can be added to the study. If the nonideal and interrupted transmission cases are considered, i.e., when the data transmission is interrupted, the latest data updates can be used to estimate target's path by extrapolation. Then, the effects on the results can be examined. Furthermore, this study has the potential for further research into sensor models, error models associated with these sensors, as well as the estimation of these errors.

- In the optimal midcourse phase, it is required to find the proper grid/knot number to obtain optimal results. Instead of trials with multiple simulations,

a “mesh refinement algorithm” can be developed to decide the proper grid number in an automatized manner.

As technology advances, the performance of the processors, into which the guidance algorithms are embedded, improves. If the processors attain significant development, that is with the integration of optimization algorithms suitable for onboard usage, the proposed guidance method could become feasible in the future.

REFERENCES

[1] “METEOR | Air Dominance, AIR SUPERIORITY | MBDA,” *MBDA*, Sep. 13, 2022. https://www.mbda-systems.com/product/meteor/

[2] “AMRAAM Missile AIM-120 By Raytheon - Advanced BVR Missile,” *World Defence News*, Dec. 16, 2023. https://www.worlddefencenews.com/amraam-missile/

[3] P. Majumdar, “Discover the Best of the Vympel R-77 Adder Missile - Prajesh Majumdar - Medium,” *Medium*, Mar. 10, 2024. [Online]. Available: https://medium.com/@AirPra/discover-the-best-of-the-vympel-r-77-adder-missile-93b50b135767

[4] J. Pike, “PL-15 air-to-air missile.”

https://premium.globalsecurity.org/military/world/china/pl-15.htm [Accessed: Sep. 17, 2024].

[5] F. Goldstein and A. Calise, "Optimal propulsion/guidance analysis of ramjet powered air-to-air missiles," in *Proceedings of the 18th IEEE Conference on Decision and Control including the Symposium on Adaptive Processes*, 1979, pp. 644-646.

[6] K. Sarkar, P. Kar, A. Mukherjee, and R. Padhi, “Range extension of an air-to-air engagement by offline trajectory optimization,” *AIAA Atmospheric Flight Mechanics Conference*, Jun. 2011, doi: 10.2514/6.2011-6339.

[7] S.-M. Hong, M.-J. Tahk, and C.-H. Lee, “Stage optimization of anti-air missiles using practical guidance laws,” *International Journal of Aeronautical and Space Sciences*, vol. 21, no. 2, pp. 394–403, Nov. 2019, doi: 10.1007/s42405-019-00224-y.

[8] M. P. Van Hoorn, “Optimizing air-to-air missile guidance using reinforcement learning”, Delft University of Technology, Delft, Netherland, 2019.

[9] Z.-H. Yang, J.-C. Fang, and Z.-Q. Qi, "Flight midcourse guidance control based on genetic algorithm," GECCO’05, June 25–29, 2005, Washington, DC, USA.

[10] Y.-L. Lee, K.-Y. Chen, and S.-J. Liao, “Using proportional navigation and a particle swarm optimization algorithm to design a dual mode guidance,” *Computers & Electrical Engineering*, vol. 54, pp. 137–146, Aug. 2016, doi: 10.1016/j.compeleceng.2016.01.025.

[11] A. D. Sanders et al., “Multi-disciplinary design of a supersonic, long-range, air-superiority missile through parametric design space exploration and physics-based modeling,” in 50th AIAA/ASME/SAE/ASEE Joint Propulsion Conference 2014, 2014. doi: 10.2514/6.2014-3603.

[12] T. Zadzora, “Formulation of the optimal trajectory for an air-breathing medium range air-to-air Missile,” 1995.

[13] M. Manickavasagam, A. K. Sarkar, and V. Vaithiyanathan, “Trajectory optimization of long range and air-to-air tactical flight vehicles,” *Defence Science Journal/Defence Science Journal*, vol. 65, no. 2, pp. 107–118, Apr. 2015, doi: 10.14429/dsj.65.8238.

[14] P. Kee, L. Dong, and C. Siong, “Near optimal midcourse guidance law for flight vehicle,” *36th AIAA Aerospace Sciences Meeting and Exhibit*, Jan. 1998, doi: 10.2514/6.1998-583.

[15] M. Kemal Özgören, “Seminar Notes on Dynamics and Control of Guided Missiles,” Ankara, Turkey, Feb. 1991.

[16] Q. Zaikang and L. Defu, *Design of Guidance and Control Systems for Tactical Missiles*. 2019.

[17] M. Kemal Özgören, *Kinematics of General Spatial Mechanical Systems*. 2020. doi: 10.1002/9781119195740.

[18] A. Kahvecioğlu, “A tool for designing robust autopilots for ramjet missiles,” M.S. - Master of Science, Middle East Technical University, 2006.

[19] Anonymous, "Specific Impulse Diagram," in *Wikimedia Commons*. [Online]. Available: https://commons.wikimedia.org/wiki/File:Specific-impulse-kk-20090105.png Accessed: Sep. 15, 2024.

[20] C. Rosema, J. Doyle, L. Auman, M. Underwood, and W. B. Blake, "Missile datcom user's manual-2011 revision," Tech. Rep., Aviation and Missile Research, Development, and Engineering Center Redstone Arsenal AL, 2011.

[21] "Manual of the ICAO Standard Atmosphere - extended to 80 kilometres / 262,500 feet (Doc 7488)," *ICAO*. https://store.icao.int/en/manual-of-the-icao-standard-atmosphere-extended-to-80-kilometres-262500-feet-doc-7488

[22] "Fit curve or surface to data - MATLAB fit."

https://www.mathworks.com/help/curvefit/fit.html

[23] P. H. Zipfel and J. A. Schetz, "Modeling and Simulation of Aerospace Vehicle Dynamics," American Institute of Aeronautics and Astronautics, Inc., 2007.

[24] Katsuhiko. Ogata, *Modern Control Engineering*. Prentice-Hall, 2010.

[25] M. Ulu, "Sliding mode guidance of an air-to-air missile," M.S. - Master of Science, Middle East Technical University, 2013.

[26] M. Kelly, "An Introduction to Trajectory Optimization: How to Do Your Own Direct Collocation," 2017. doi: 10.1137/16M1062569.

[27] M. P. Kelly, “Transcription Methods for Trajectory Optimization,” Feb. 2015.

[28] J. T. Betts, *Practical Methods for Optimal Control and Estimation Using Nonlinear Programming*. Society for Industrial and Applied Mathematics, 2010.

[29] “Find minimum of constrained nonlinear multivariable function - MATLAB fmincon.” https://www.mathworks.com/help/optim/ug/fmincon.html

[30] R. Yanushevsky, *Modern Missile Guidance*. CRC Press, 2008. [Online]. Available: http://www.crcpress.com

[31] A. P. Australia and A. P. Australia, “Grisha’s Missile \xc2\xabShoot-Off\xc2\xbb.” https://www.ausairpower.net/APA-NOTAM-200408-1.html

[32] C. Let, *The Use of Differential Geometry to Control and Guidance*. [Online]. Available: https://slideplayer.com/slide/12359342/

[33] J. Stillion *et al.*, “Trends in air-to-air combat implications for future air superiority,” Center for Strategic and Budgetary Assessments, 2015.